Neuron

Article

Subunit composition, molecular environment, and activation of native TRPC channels encoded by their *interactomes*

Graphical abstract

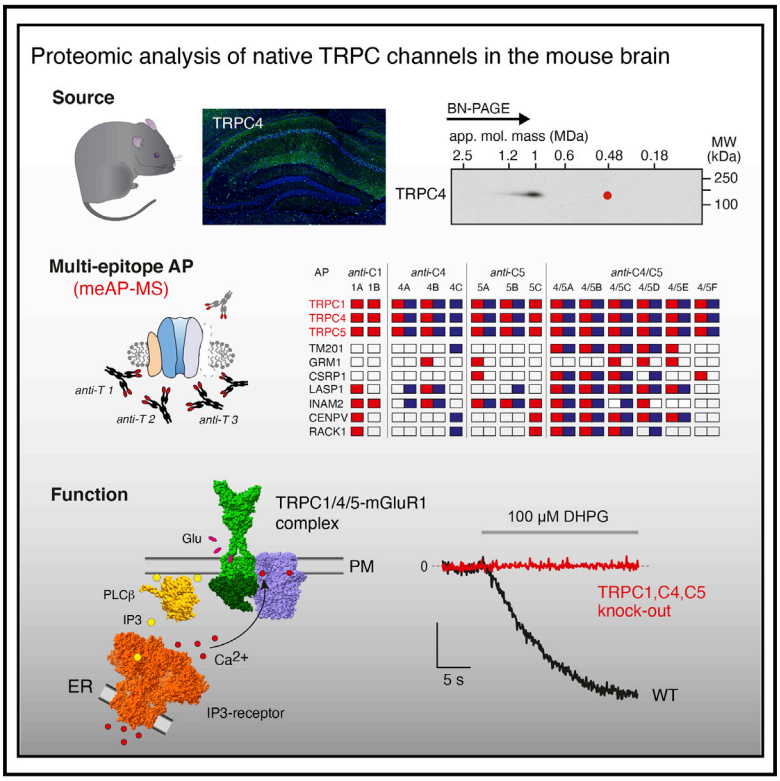

Highlights

- TRPC channels in the brain are macro-molecular complexes of more than 1 MDa in size
- TRPC1, C4, and C5-containing channels are heteromers; TRPC3, C6, and C7 form mostly homomers
- TRPC1/C4/C5 channels co-assemble with the metabotropic glutamate receptor mGluR1
- Receptor-channel complexes render channel activation both specific and reliable

Authors

Astrid Kollewe, Yvonne Schwarz, Katharina Oleinikov, ..., Dieter Bruns, Veit Flockerzi, Bernd Fakler

Correspondence

veit.flockerzi@uks.eu (V.F.), bernd.fakler@physiologie.uni-freiburg.de (B.F.)

In brief

TRPC channels are critical for a variety of processes in the mammalian brain, from neuronal growth and synaptogenesis to transmitter release, synaptic transmission, and plasticity. Kollewe et al. show that native TRPC channels are macro-molecular complexes whose assembly and operation is defined by their interactomes.

Kollewe et al., 2022, Neuron *110*, 1–14
December 21, 2022
https://doi.org/10.1016/j.neuron.2022.09.029

CellPress

Neuron

CellPress

Article

Subunit composition, molecular environment, and activation of native TRPC channels encoded by their *interactomes*

Astrid Kollewe,[1] Yvonne Schwarz,[2] Katharina Oleinikov,[2] Ahsan Raza,[3] Alexander Haupt,[1] Philipp Wartenberg,[3] Amanda Wyatt,[3] Ulrich Boehm,[3] Fabien Ectors,[4] Wolfgang Bildl,[1] Gerd Zolles,[1] Uwe Schulte,[1,5] Dieter Bruns,[2] Veit Flockerzi,[3,*] and Bernd Fakler[1,5,6,7,*]

[1]Institute of Physiology, Faculty of Medicine, University of Freiburg, Hermann-Herder-Str. 7, 79104 Freiburg, Germany
[2]Institute of Physiology, Center for Integrative Physiology and Molecular Medicine, Saarland University, 66421 Homburg, Germany
[3]Experimental and Clinical Pharmacology and Toxicology, PZMS, Saarland University, 66421 Homburg, Germany
[4]Transgenic facility, FARAH Research Center, Faculty of Veterinary Medicine, University of Liège, 4000 Liège, Belgium
[5]Signalling Research Centres BIOSS and CIBSS, Schänzlestr. 18, 79104 Freiburg, Germany
[6]Center for Basics in NeuroModulation, Breisacherstr. 4, 79106 Freiburg, Germany
[7]Lead contact
*Correspondence: veit.flockerzi@uks.eu (V.F.), bernd.fakler@physiologie.uni-freiburg.de (B.F.)
https://doi.org/10.1016/j.neuron.2022.09.029

SUMMARY

In the mammalian brain TRPC channels, a family of Ca^{2+}-permeable cation channels, are involved in a variety of processes from neuronal growth and synapse formation to transmitter release, synaptic transmission and plasticity. The molecular appearance and operation of native TRPC channels, however, remained poorly understood. Here, we used high-resolution proteomics to show that TRPC channels in the rodent brain are macro-molecular complexes of more than 1 MDa in size that result from the co-assembly of the tetrameric channel core with an ensemble of interacting proteins (*interactome*). The core(s) of TRPC1-, C4-, and C5-containing channels are mostly heteromers with defined stoichiometries for each subtype, whereas TRPC3, C6, and C7 preferentially form homomers. In addition, TRPC1/C4/C5 channels may co-assemble with the metabotropic glutamate receptor mGluR1, thus guaranteeing both specificity and reliability of channel activation via the phospholipase-Ca^{2+} pathway. Our results unveil the subunit composition of native TRPC channels and resolve the molecular details underlying their activation.

INTRODUCTION

Transient receptor potential canonical (TRPC) channels participate in a broad range of physiological processes in a wide variety of tissues and cell types (Freichel et al., 2005; Kirtley et al., 2021).

In rodents, the TRPC family consists of seven members (TRPC1–7) which, based on sequence similarity, can be divided into three subgroups TRPC1, C4, C5, TRPC3, C6, C7, and TRPC2 (Blair, 2021; Figure 1A), a pseudogene in humans. Although some TRPC proteins are broadly expressed (TRPC1), others are preferentially found in a limited number of tissues (TRPC3, TRPC5, and TRPC7). All of them, however, are expressed in the brain, where they have been implicated in a plethora of functions ranging from neuronal growth and spine/synapse formation to transmitter release, synaptic transmission, and plasticity. Their impairment is linked to neurological diseases (Fogel et al., 2015; Jeon et al., 2020; Selvaraj et al., 2010; Wang et al., 2017).

As tetrameric assemblies, TRPCs operate as non-selective cation channels that are permeable to calcium (Ca^{2+}) and monovalent cations and, hence, upon activation can signal through depolarization of the membrane potential and/or through increasing the intracellular Ca^{2+} concentration. Each TRPC subunit contains six transmembrane (TM) domains (S1–S6), a pore loop domain between S5 and S6, and extended cytoplasmic N and C termini (Gaudet, 2008) with multiple domains implicated in subunit tetramerization, control of channel gating, and potential interactions with partner proteins (Bai et al., 2020; Duan et al., 2018; Myeong et al., 2016; Sierra-Valdez et al., 2018; Song et al., 2021; Tang et al., 2018; Vinayagam et al., 2018; Wright et al., 2020). In addition, combination of subunits into homo- or hetero-tetramers modifies channel properties such as Ca^{2+} permeability, sensitivity to phosphatidylinositol-4,5-bisphosphate (PIP_2) hydrolysis, and shape of the current voltage (I-V) relationship (Kim et al., 2014; Ko et al., 2017, 2019; Lintschinger et al., 2000; Maruyama et al., 2006; Storch et al., 2012; Strübing et al., 2001). Although all TRPC channels can be activated upon stimulation of G-protein-coupled receptors (GPCRs) via metabolites downstream of phospholipase C signaling, the exact mechanism of activation or modes of regulation are

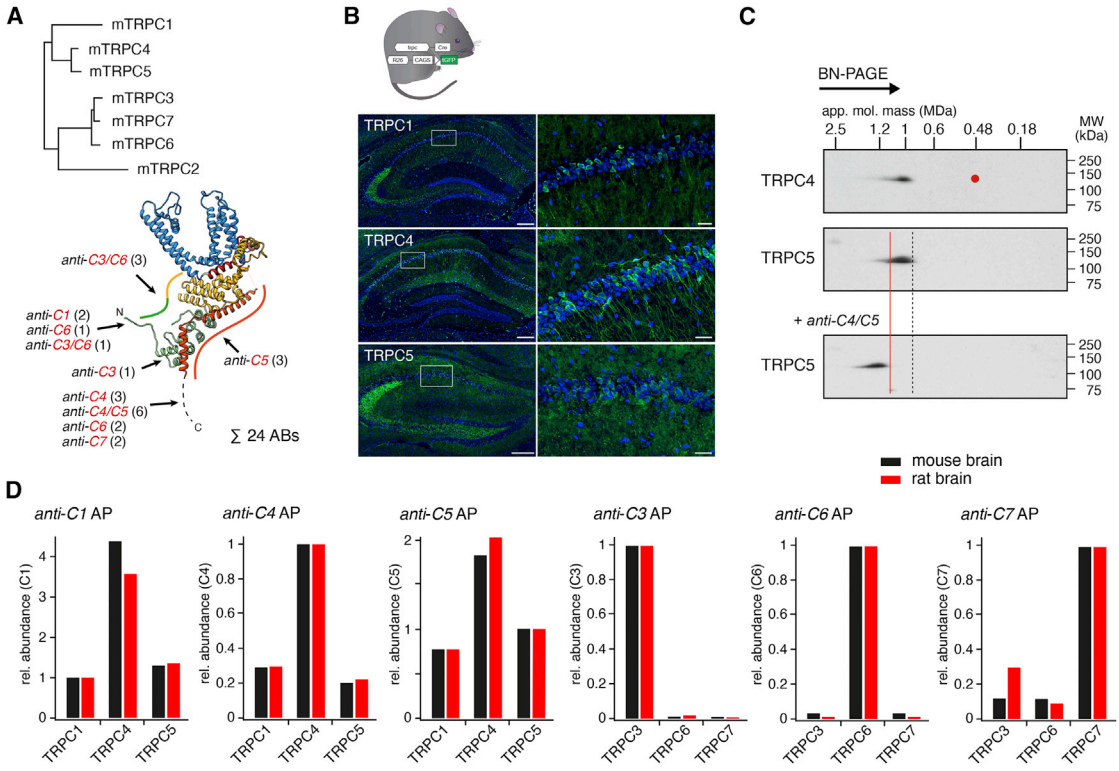

Figure 1. Native TRPC channels in the rodent brain are macro-molecular complexes

(A) Upper panel: unrooted phylogenetic tree generated for mouse TRPC1-7 amino acid sequences using MAFFT (v7.471) with standard settings. Lower panel: epitope projection of the *anti-TRPC* ABs used in this study onto the 3D-structure of a single TRPC4 subunit (Vinayagam et al., 2018). Number of ABs targeting similar sites is given in parenthesis. Isoform-specific ABs are written as *anti-Cx*, and ABs binding several TRPC isoforms are labeled as *anti-Cx/Cy*. Color coding is as follows: green (ankyrin repeat domain), yellow (helical linker and pre S1 domains), blue (channel domain), red (TRP domain, Rib helix, and calmodulin- and IP_3 receptor-binding [CIRB] site). See also Table S1.

(B) Expression of TRPC1, C4, C5 in the hippocampal formation of reporter mice (top). Frames indicate region(s) magnified on the right. Green: GFP fluorescence of TRPC reporter, blue: DAPI stain of nuclei; scale bars are 200 and 25 μm, respectively.

(C) Two-dimensional gel separation of a CL-47 solubilized membrane fraction from rodent brain without (top and middle panel) or after preincubation with *anti-TRPC4/C5* (4/5A) (bottom panel) and Western probed with the indicated ABs. Apparent molecular mass (BN-PAGE) and molecular weight are as indicated, and red dot marks predicted mass of a TRPC tetramer. See also Figure S5.

(D) Molecular abundance of co-purified TRPC isoforms relative to target in APs with isoform-specific ABs and CL-91 solubilized membrane fractions from mouse (red) or rat (black) brain. Note extensive heteromerization between TRPC1, C4, and C5 isoforms and lack thereof for TRPC3, C6, and C7.

controversially discussed. They may vary between different TRPC family members and depend on the cellular environment or assay conditions (reviewed by Venkatachalam and Montell, 2007 and Wang et al., 2020). Receptor and store operated mechanisms have been described including activation by an increase in cytosolic Ca^{2+} or 1,2-diacylglycerol (DAG) (Blair et al., 2009; Gross et al., 2009; Hofmann et al., 1999; Venkatachalam et al., 2003), through conformational changes based on direct interactions of TRPCs with inositol-1,4,5-trisphosphate receptors (IP_3R), STIM, or Orai (Huang et al., 2006; Kiselyov et al., 1999; Lee et al., 2010, 2014; Tang et al., 2001; Yuan et al., 2009; Zhang et al., 2001) and the insertion of TRPC channels into the plasma membrane upon vesicle exocytosis (Bezzerides et al., 2004; Cerny and Huber, 2011; Tai et al., 2011).

Many of these modes of action have been derived from heterologously expressed TRPCs, whereas molecular information about assembly and function of native TRPC channels is limited and respective investigations have been precluded by technical difficulties and low expression levels (Flockerzi et al., 2005; Montell, 2005; Zheng and Phelan, 2014). These obstacles can be overcome, though, by high-resolution proteomics that combine affinity-purification of native proteins/protein complexes with nano-flow liquid chromatography tandem mass spectrometry (nano-LC-MS/MS) and that were successfully used to unravel subunit composition and operation of a number of native ion channels, transporters, and receptors (Kollewe et al., 2021; Schmidt et al., 2017; Schwenk et al., 2010, 2012, 2016, 2019).

Here, we applied this proteomic workflow to unveil the molecular appearance of native TRPC channels in the rodent brain. We show that native TRPC channels are macro-molecular complexes with an apparent size of around 1 MDa and uncovered distinct homomer and heteromer formation among the TRPC family members. Moreover, we resolved the interactome(s) of native TRPC channels and identified direct interaction between TRPC1/C4/C5 channels and the metabotropic glutamate receptor 1 (mGluR1). Subsequent functional studies demonstrated the

significance of the receptor-channel assembly for robust agonist-triggered activation.

RESULTS

Native TRPC channels are macro-molecular complexes

For thorough investigation of molecular appearance and function of TRPC channels and the distinctness of the various TRPC isoforms, we set out to determine the subunit composition of TRPC channels in native tissue. As a source, we used membrane fractions prepared from whole brains of adult mice where expression of all TRPC family members has been described (Chen et al., 2017; Riccio et al., 2002). Moreover, gene-specific GFP-reporter mice (Wyatt et al., 2017) unraveled robust co-expression of TRPCs 1, 4, and 5 in the same cell types, as illustrated for pyramidal neurons in the CA1 region of the hippocampus (Figure 1B, right panel) in line with previous findings (Chung et al., 2006).

First investigations of the aforementioned membrane fractions by native gel electrophoresis (BN-PAGE) showed that TRPC4 and TRPC5 containing channels in the rodent brain are high-molecular-weight complexes of approximately 1 MDa, considerably exceeding the size anticipated for the respective TRPC tetramers (~450 kDa, Figure 1C). These results suggested that native TRPC4 and TRPC5 channels are more complex assemblies than plain tetramers and that these assemblies are well preserved during solubilization with the mild detergent CL-47 (Kollewe et al., 2021; Müller et al., 2010; Schmidt et al., 2017; Schwenk et al., 2010, 2012, 2016). Noteworthy, all TRPC4, 5 containing complexes were shifted on native gels by addition of an antibody (AB) targeting both TRPC isoforms, thus confirming the specificity of the Western-blot signal (Figure 1C, bottom).

For determination of the subunit composition of native TRPC assemblies, we next performed multi-epitope affinity purifications (meAPs; Kollewe et al., 2021; Schmidt et al., 2017; Schwenk et al., 2012, 2016, 2019) on solubilized membrane fractions from brains of adult rats and mice utilizing ABs that targeted each member of the TRPC family except TRPC2. In preparation for these experiments, we tested a number of commercial and custom-made *anti-TRPC* ABs for both their efficiency and their target-specificity in APs; for the latter, we used source material from either single (TRPC1,3-7) or triple (TRPC1,C4,C5 or TRPC3,C6,C7) target knockout animals. These efforts finally identified a total of 24 ABs suited for efficient AP of TRPC proteins. Important to note, the epitopes of these ABs were either isoform specific or present in a subset of TRPC proteins and located at various positions along the primary sequences of the TRPC isoforms (Figure 1A; details in Table S1). The latter reduced experimental biases introduced by selective binding properties of individual ABs or individual epitopes. In addition, probing detergent buffers of different stringency showed that the previously established buffer systems CL-47 (mild stringency) and CL-91 (intermediate stringency) effectively solubilized the TRPC proteins, albeit with isoform-specific differences (Figure S1).

The eluates of all APs performed with the selected set of 24 ABs on membrane fractions solubilized under either condition were subjected to high-resolution liquid mass spectrometry (nano-LC-MS/MS) and analyzed by label-free peak volume-based quantification to determine identity and amount of the precipitated proteins (Bildl et al., 2012; Kollewe et al., 2021; Schmidt et al., 2017; Schwenk et al., 2019). The data confirmed effective purification of the TRPC target proteins reflected by relative coverages of 41.6% (TRPC1), 63.4% (TRPC3), 63.0% (TRPC4), 46.5% (TRPC5), 53.4% (TRPC6), and 34.2% (TRPC7) of the primary sequences by MS/MS-identified peptides (Figure S2). In addition, the meAP-experiments exposed distinct preferences of individual TRPC isoforms for formation of homomeric or heteromeric tetramers and identified a number of proteins that co-assemble with TRPC tetramers to form the high-molecular-weight channel complexes in the rodent brain, including several proteins that have not yet been associated with TRPC channel function(s).

Distinct formation of heteromultimers between TRPC family members

Quantitative analysis of the subset of APs utilizing isoform-specific *anti-TRPC1*, *anti-TRPC4*, and *anti-TRPC5* ABs provided a number of details on the multimerization of the TRPC proteins in the rodent brain (Figure 1D). First, TRPC1, C4, and C5 robustly co-assemble into heteromers with each other in both rats and mice, in line with a previous report from hippocampus (Bröker-Lai et al., 2017). Second, in these heteromers, the amount of TRPC4 exceeds that of TRPC1 and TRPC5 as indicated by the abundance values determined in all *anti-TRPC1*, *C4*, *C5* APs independent of the respective target protein and the rodent species (Figure 1D, three left panels). Third, the vast majority of TRPC3 (97%), TRPC6 (94%), and TRPC7 (77%) appears in homomeric configuration, whereas only minor portions are integrated into heteromers with each other, most likely as a result of restricted co-expression. Fourth, the total amount of TRPC3 exceeded that of TRPCs 6 and 7 by roughly 10-fold and 20-fold, respectively (data not shown). Fifth, no heteromerization was observed beyond the TRPC1/C4/C5 or TRPC3/C6/C7 subgroups.

TRPC1, C4, and C5 form hetero-tetramers with defined subunit stoichiometries

To resolve and quantify the natively formed heteromer populations assembled from TRPC1, C4, and C5, we performed sequential APs using isoform-specific *anti-TRPC1*, *anti-TRPC4*, and *anti-TRPC5* ABs in every order possible. This experimental set-up is exemplified in Figure 2A (left panel) for a series starting with *anti-TRPC1*: after precipitation of all TRPC1-containing complexes via *anti-TRPC1* AP, the supernatant was equilibrated with *anti-TRPC4* ABs to precipitate remaining TRPC4 and associated TRPC5 (left string) or *anti-TRPC5* ABs to precipitate remaining TRPC5 and associated TRPC4 (right string). In a third round homomeric TRPC5 (left string) or homomeric TRPC4 (right string) that were not captured in the previous rounds were precipitated with *anti-TRPC5* and *anti-TRPC4* ABs, respectively. The amounts of TRPC proteins determined in each sample by nano-LC-MS/MS were finally combined to deduce the abundance of each isoform in all possible homo- and hetero-tetrameric configurations by solving an overdetermined system of linear equations (see STAR Methods and Table S2). The

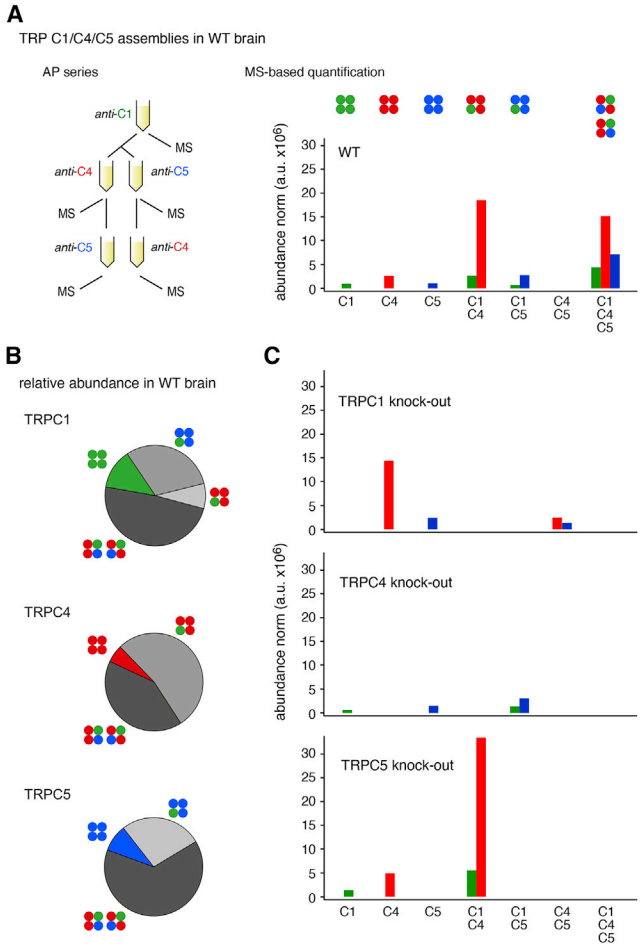

Figure 2. Molecular appearance of TRPC1, C4, C5 channels in the rodent brain

(A) Left panel: scheme illustrating an example of serial APs with ABs specific for TRPC1, TRPC4, and TRPC5 isoforms and CL-91 solubilized membrane fractions from mouse brain followed by quantitative MS/MS analysis. Right panel: molecular abundance of TRPC1, TRPC4, and TRPC5 present in homo- and heteromeric assemblies in WT mouse brain. Suggested subunit stoichiometries are indicated on the top.

(B) Relative abundance of each isoform in homomeric (colored) or heteromeric (gray, pictograms as in 2A, right panel) assemblies in WT mouse brain.

(C) Molecular abundance of TRPC1, TRPC4, and TRPC5 in homo- and heteromeric complexes in brains of mice with a genetic deletion of the indicated TRPC isoform.

See also Table S2.

outcome, summarized in Figures 2A (right panel) and 2B, unveiled several unexpected findings. Thus, only minor portions of the TRPC1, TRPC4, and TRPC5 proteins in the brain are present in homomers (13%, 6%, and 9%, respectively, Figure 2B), whereas the majority is integrated into three types of heteromers: TRPC1/C4, TRPC1/C5, and TRPC1/C4/C5 (Figures 2A and 2B). TRPC1-free heteromers were not detected. In addition, the abundance values determined for the three isoforms in the three different hetero-tetramers suggested defined stoichiometries of 1:3 for TRPC1/C4 and TRPC1/C5 and of 1:2:1 for the triple TRPC1/C4/C5 heteromer (Figure 2A, right panel).

These defined TRPC assemblies were further investigated by recapitulating serial APs with membrane fractions prepared from mice with genetic deletions of the individual TRPC1, 4, 5 proteins. MS-based quantification showed that in all cases, the knockout of the target protein did not lead to a compensatory increase in expression of the remaining TRPC proteins but rather to a reduction of their overall amounts and to considerable changes in their allocation to homomers and heteromers (Figure 2C). Specifically, knockout of TRPC1 decreased the amounts of TRPC4 and TRPC5 by 56% and 67%, respectively. Moreover, none of the heteromeric assemblies observed in WT were detected. Instead homomeric TRPC4 and TRPC5 assemblies were increased in abundance (by roughly 2-fold to 5-fold), and small amounts of TRPC4/C5 heteromers were identified (Figure 2C, upper panel). Knockout of TRPC4 resulted in a profound reduction of TRPC1 and TRPC5 amounts by 80% and 58%, respectively, whereas TRPC4-free assemblies appeared largely unaltered (Figure 2C, middle panel). In contrast, deletion of TRPC5 had the least effect on overall amounts of the remainders (TRPC1 decreased by 20%; TRPC4 increased by 7%) but augmented the amount of TRPC1/C4 heteromers by about 2-fold (Figure 2C, lower panel).

Together, these results indicated that stability and subunit stoichiometry of heteromers assembled from TRPC1, C4, and C5 are predominantly determined by the TRPC1 subunit. Interestingly, the TRPC1/C4 heteromer is strongly preferred over the TRPC1/C5 combination.

Interactomes of native TRPC channel complexes

For comprehensive determination of proteins that co-assemble with the TRPC tetramers to form the high-molecular-weight complexes present in the brain (Figure 1C), all of the 1,080–1,370 proteins identified in the various meAPs by nano-LC-MS/MS were scrutinized for their specific and consistent co-purification with TRPCs (see also STAR Methods). Specificity was assessed by comparing the enrichment of each co-purified protein in APs from WT with target knockout material (target-normalized ratio [tnR]; see STAR Methods). In this context, mice with deletions of individual TRPC genes were used as negative controls for isoform-specific ABs, whereas TRPC1, C4, C5, and TRPC3, C6, C7 triple-knockout mice were used in experiments with ABs targeting TRPC4 and TRPC5 or TRPC3 and TRPC6, respectively. Consistency was judged from the number of APs in which a given protein was dubbed specifically co-purified (Müller et al., 2010; Schwenk et al., 2012, 2016); this criterion was considered met with at least four *anti-TRPC1*, *anti-TRPC4*, or *anti-TRPC5* APs for TRPCs 1, 4, 5 (analyzed together based on their extensive heteromer formation), with at least two *anti-TRPC6* APs and with two *anti-TRPC7* APs (further details in STAR Methods) for TRPC6 and TRPC7, respectively.

Application of these criteria to the large series of meAPs delineated distinct interactomes, the entirety of interacting proteins, for the aforementioned subgroups of TRPCs (Figure 3; Tables 1, 2, and S3). Accordingly, 15 proteins that all specifically and consistently co-purified with TRPC1, C4, and C5 were classified as constituents of the TRPC1/C4/C5 interactome (Table 1); most of them have not yet been related to TRPC function and/or cell biology. Structurally, these interactome constituents span a wide range

Please cite this article in press as: Kollewe et al., Subunit composition, molecular environment, and activation of native TRPC channels encoded by their *interactomes*, Neuron (2022), https://doi.org/10.1016/j.neuron.2022.09.029

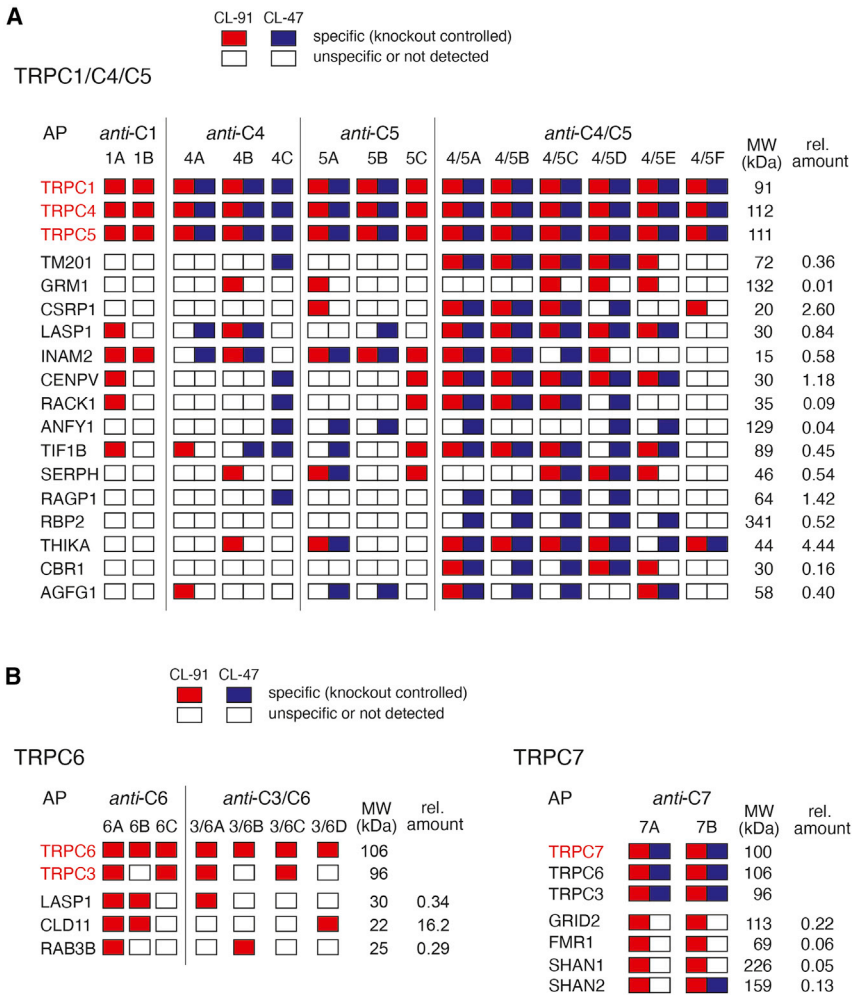

Figure 3. Protein constituents of native TRPC channel complexes in the mouse brain

Tables summarizing the results of all APs with ABs targeting TRPC1, TRPC4 or TRPC5 (A), and TRPC6 (B, left panel) or TRPC7 (B, right panel). Top row indicates specificity of ABs, and second row is AB referencing. Color coding as indicated. Molecular weight and maximal molecular abundance per TRPC tetramer are shown on the right.

See also Table S3.

in MW (~15–350 kDa) and, in (various) combination(s), reconstitute the high-molecular-weight assemblies observed in membrane fractions from rodent brain (Figure 1C), in contrast to heterologously expressed (sole) channels (Figure S5A). The identified interactors were either (soluble) cytoplasmic proteins (12 of 15) or TM proteins (3 of 15). The latter included the metabotropic glutamate receptor 1 (mGluR1 or GRM1), the multispan-membrane protein TM201 and the one-TM domain protein INAM2, a homolog of the InaF-locus proteins first described as TRP-interactors/modulators in flies (Chen and Montell, 2020; Cheng and Nash, 2007; Li et al., 1999; Rosenzweig et al., 2008). The soluble interactome constituents comprise several proteins implied in scaffolding or cytoskeleton function (LASP1, RACK1, and RAGP1), proteins with enzymatic activity (RBP2, THIKA, CBR1 and TIF1B), as well as proteins that are implied in protein processing/trafficking or currently lack annotation of primary functions (CSRP, AGFG1, and ANFY1). It should be noted that efficiency of co-purification (rel. abundance/amount in Figure 3 and Tables 1 and 2) is a combined effect of physical interaction and susceptibility to detergent buffers (Schwenk et al., 2012, 2016); it does not faithfully reflect the degree of association under cellular conditions nor the physiological significance *in-vivo*.

For TRPC6 and TRPC7, fewer interactors could be assigned as a combined result of the rather low target protein expression, solubilization characteristics (TRPC6 is hardly soluble at CL-47), and the efficiency of the respective ABs. Notwithstanding, TRPC6 was found to specifically co-assemble with TRPC3 and proteins LASP1, Claudin 11, and Rab3B, whereas TRPC7 associated with the postsynaptic scaffold proteins Shank1 and 2, as well as GRID2 and FMR1, in addition to TRPC3 and TRPC6 (Figure 3B; Table 2). Determination of a TRPC3 interactome was precluded by the availability of only one isoform-specific AB.

Together, the interactomes demonstrated that TRPC channels in the mammalian brain are macro-molecular assemblies of variable, but distinct subunit composition rather than uniform complexes or plain tetramers very similar to other membrane proteins such as TRPM7 channels, AMPA-type glutamate receptors, or metabotropic GABA ($GABA_B$) receptors (Kollewe et al., 2021; Schwenk et al., 2012, 2016).

Operation of macro-molecular TRPC-receptor complexes

Intrigued by the consistent co-purification of mGluR1-type GPCRs with TRPC1/C4/C5 channels despite the high sensitivity of GPCR-co-assemblies to detergent buffers, we decided to further investigate this interaction, which may represent a mode for reliable channel activation by released glutamate as previously suggested (Dong et al., 2009; El-Hassar et al., 2011; Gee et al., 2003; Kim et al., 2003; Zhang et al., 2001).

In the first step, we probed stable formation of channel-receptor complexes in heterologous systems via transient expression of HA-tagged mGluR1 with TRPC1, TRPC4, and TRPC5 in HEK293 cells. Subsequent APs using either *anti-HA* or *anti-TRPC* ABs resulted in efficient co-purification of both interaction partners in all APs (Figure 4A), strongly suggesting direct binding between the mGluR1 receptors and TRPC1/C4/C5 channels. This binding mostly likely occurs through the TM domains as TRPC1/C4/C5 channels also co-purified a splice-variation of mGluR1 that lacks most of the cytoplasmic

Please cite this article in press as: Kollewe et al., Subunit composition, molecular environment, and activation of native TRPC channels encoded by their *interactomes*, Neuron (2022), https://doi.org/10.1016/j.neuron.2022.09.029

Table 1. Protein constituents of native TRPC1, C4, C5-containing complexes in mouse brain identified by meAPs

ID	Acc. no.	Name	Alternative name(s)	Function	rel. abundance CL-91	rel. abundance CL-47
TRPC1	Q61056	TRP channel C1	–	ion channel	<	<
TRPC4	Q9QUQ5	TRP channel C4	–	ion channel	=	=
TRPC5	Q9QX29	TRP channel C5	–	ion channel	<	=
TM201	A2A8U2	Transmembrane protein 201	–	unknown	<<	=
GRM1	P97772	metabotropic glutamate receptor 1 (mGluR1)	–	GPCR	<<	–
CSRP1	P97315	Cysteine and glycine-rich protein 1	–	unknown	=	=
LASP1	Q61792	LIM and SH3 domain protein 1	MLN 50	adaptor, cytoskeleton	<	=
INAM2	P0DMQ5	Transmembrane protein INAFM2	–	regulatory protein	<	=
CENPV	Q9CXS4	Centromere protein V	Prolin-rich protein 6	scaffold protein, cytoskeleton	<	=
RACK1	P68040	receptor of activated protein C kinase 1	p205, 12–3	scaffold protein	<	<
ANFY1	Q810B6	Rabankyrin-5	rank-5	endosomal trafficking	–	<<
TIF1B	Q62318	transcription intermediary factor 1-beta	E3 SUMO-protein ligase TRIM28	transcription regulation	–	=
SERPH	P19324	Serpin H1	47 kDa HSP, collagen-binding protein	chaperone, collagen	=	–
RAGP1	P46061	Ran GTPase-activating protein 1	RanGAP1	GTPase activator	–	=
RBP2	Q9ERU9	E3 SUMO-protein ligase RanBP2	Ran-binding protein 2, Nup358	Enzyme	–	=
THIKA	Q921H8	3-ketoacyl-CoA thiolase A	acetyl-CoA acyltransferase	Enzyme	=	>
CBR1	P48758	carbonylreductase	–	Enzyme	–	<
AGFG1	Q8K2K6	Arf-GAP domain and FG repeat-containing protein	nucleoporin-like protein RIP	Unknown	–	=

Accession numbers refer to the UniProtKB/SwissProt database. Relative abundances are given for the sample with the highest abundance of the respective protein. For TRPC isoforms abundances were determined relative to the overall amount of TRPC proteins in the same sample, and for all other proteins, abundances were calculated per TRPC tetramer. Relative abundances were classified as follows: > when above 3.3-fold, = when between 0.33- and 3.3-fold, < when between 0.033- and 0.33-fold, and << when between 0.0033- and 0.033-fold.

C-terminal domain(s) with similar efficiency (Figure S6). In the second step, we used the transiently transfected cells for functional measurements by whole-cell patch-clamp recordings. Figure 4B shows representative current traces recorded in response to application of the mGluR1 agonist (S)-3,5-dihydroxyphenylglycine (DHPG, 100 μM) in cells expressing mGluR1 either alone or together with various configurations of TRPC1, C4, and C5 channels (Figure 4B). In all cases, DHPG application triggered robust and transient currents of similar amplitude(s) mediated by the TRPC channels (Figure 4C). In the third step, we turned to the mode of coupling between receptor and channel parts of the complexes by distinctly interfering with the mGluR1-activated G_q-protein pathway (Wettschureck and Offermanns, 2005). Here, we probed its sensitivity to the intracellular Ca^{2+}-buffers EGTA and BAPTA which, due to their distinct binding kinetics, differentially affected functional coupling (mediated by Ca^{2+} ions) in BK_{Ca}-Cav channel-channel complexes (Berkefeld and Fakler, 2013; Berkefeld et al., 2006). In fact, intracellular BAPTA perfused at 10-mM concentration through the patch-pipette completely abolished the DHPG-triggered TRPC currents irrespective of the channels' subunit composition in contrast to 10 mM EGTA that left the current amplitudes unaffected (Figures 4D–4F). Similarly, channel activation could be completely abolished by preincubation of the cells with U-73122 (5 μM), an inhibitor of PLCβ, the established primary effector of the G_q-pathway (Wettschureck and Offermanns, 2005). These results indicated that receptor-triggered activation of TRPC channels requires Ca^{2+} ions that are released from a closely co-localized source (within a tens of nanometer distance (Fakler and Adelman, 2008)) and that most likely act through direct binding to the channel protein. This assumption was further tested in excised inside-out patches combined with fast piezo-driven Ca^{2+} application and in mutant TRPC5 channels where the three residues essential for coordinating Ca^{2+} -binding were exchanged (TRPC5-mut: E418Q, E421Q, and D439N), (Duan et al., 2019; Vinayagam et al., 2020). In inside-out patches excised from Xenopus oocytes expressing TRPC4 or TRPC1/C4/C5 channels application and withdrawal of 10 μM Ca^{2+} triggered rapid opening and closing of the channels (with ms time constants), respectively (Figure 5A); no currents were observed in the absence of Ca^{2+}. Determination of Ca^{2+} dose-response relations showed that both types of channels exhibited half-maximal activation at sub-micromolar Ca^{2+} (values for EC_{50} and Hill-coefficient of 0.65 μM and 1.7 for TRPC4 and 0.74 μM and 1.8 for TRPC1/C4/C5 obtained from fits to the mean of 4 and 5 patches). Comparative whole-cell current recordings from HEK293 cells (transiently) co-expressing mGluR1 with either TRPC5 WT or

Please cite this article in press as: Kollewe et al., Subunit composition, molecular environment, and activation of native TRPC channels encoded by their *interactomes*, Neuron (2022), https://doi.org/10.1016/j.neuron.2022.09.029

Table 2. Protein constituents of native TRPC6- or TRPC7-containing complexes in mouse brain identified by meAPs

ID	Acc. no.	Name	Alternative name(s)	Function	rel. abundance CL-91	rel. abundance CL-47
TRPC6	Q61143	TRP channel C6	–	ion channel	=	–
TRPC3	Q9QZC1	TRP channel C3	–	ion channel	<<	–
CLD11	Q99P82	Claudin-11	–	cell adhesion	>	–
LASP1	Q61792	LIM and SH3 domain protein 1	MLN 50	adaptor, cytoskeleton	=	–
RAB3B	Q9CZT8	Ras-related protein Rab-3B	–	trafficking	<	–
TRPC7	Q9WVC5	TRP channel C7	–	ion channel	=	=
TRPC6	Q61143	TRP channel C6	–	ion channel	<	<
TRPC3	Q9QZC1	TRP channel C3	–	ion channel	<	<
GRID2	Q61625	Glutamate receptor delta-2	–	unknown	<	–
FMR1	P35922	synaptic functional regulator FMR1	Fragile X mental retardation protein 1	unknown	<	–
SHAN1	D3YZU1	SH3 and multiple ankyrin repeat domains protein 1	Shank1	scaffold protein	<	–
SHAN2	Q80Z38	SH3 and multiple ankyrin repeat domains protein 2	Shank2	scaffold protein	<	–

Accession numbers refer to the UniProtKB/SwissProt database. Relative abundances are given for the sample with the highest abundance of the respective protein. For TRPC isoforms abundances were determined relative to the overall amount of TRPC proteins in the same sample, and for all other proteins, abundances were calculated per TRPC tetramer. Relative abundances were classified as follows: > when above 3.3-fold, = when between 0.33- and 3.3-fold, < when between 0.033- and 0.33-fold, and << when between 0.0033- and 0.033-fold.

TRPC5-mut channels showed that Ca^{2+}-binding to the TRPC protein is required for channel activation: While robust transient currents were observed upon DHPG application with TRPC5 WT, no currents could be determined with TRPC5-mut, although the mutated protein was robustly expressed and inserted in the plasma membrane (Figure 5B).

Finally, we assessed native TRPC-mGluR1 complexes expressed in autaptic cultures of hippocampal neurons from both WT (selected for TRPC5 expression via the τGFP-reporter) and TRPC1, C4, C5 triple-knockout mice (Figure 6A, upper panel). As shown in Figure 6A, bath application of 100 μM DHPG to such cultures triggered robust inward currents (with rapid onset) in WT neurons held at a membrane potential of −70 mV in whole-cell recordings that were absent in triple-knockout neurons (Figures 6A, lower panel and 6B).

Together, these results indicated that TRPC-mGluR complexes give rise to robust cation currents that are effectively activated by intracellular Ca^{2+} delivered through the PLC-pathway after activation of their GPCR moiety by agonist binding. Subsequent to channel activation, the increased intracellular Ca^{2+} concentration may lead to a complete closure of the channels most likely via Ca^{2+}-dependent binding of calmodulin to the calmodulin- and IP_3 receptor-binding (CIRB) domain as recently suggested from 3D-structures of TRPC4 (Vinayagam et al., 2020).

DISCUSSION

In this work, we show that native TRPC channels in the mammalian brain are not plain tetramers but rather macro-molecular assemblies whose subunit composition and diversity is defined by their subtype-specific interactomes. The respective constituents define the architecture of the homomeric and heteromeric channel pore(s) and determine mode and specificity of channel activation and other aspects underlying the cell physiological significance of this family of TRP channels.

Molecular appearance of native TRPC channels in the brain

For thorough analysis of the molecular appearance and the protein building blocks of native TRPC channels in the mammalian brain, we applied our established proteomic approach with native gel separation, series of meAPs, and quantitative high-resolution MS analysis (Schmidt et al., 2017; Schwenk et al., 2010, 2012, 2016, 2019). These analyses unveiled native TRPC channels as high-molecular-weight assemblies (Figure 1) that largely outweigh plain tetramers of the pore-forming subunits often referred to as TRPC channel(s) and that result from co-assembly of tetrameric core(s) with an ensemble of peripheral subunits. A similar macro-molecular arrangement was recently identified for native TRPM7 in mouse brain (Kollewe et al., 2021) and HEK-cells (Bai et al., 2021), suggesting a more general feature for the appearance of TRP channels in native tissue.

Detailed investigation of the tetrameric TRPC cores by meAP and serial AP experiments (Figures 1 and 2) uncovered quite distinct architecture(s) for the two subclasses in the TRPC family (Blair, 2021): TRPC1, C4, C5 are built as hetero-tetramers (see below), whereas TRPC3, C6, C7 are mostly made up as homomers. Notwithstanding, the latter is not due to structural constraints but rather due to restricted co-expression patterns, as suggested by the small, but detectable amount of TRPC3/C6/C7 heteromers (Figure 1, *anti-TRPC7* AP). It must be

Please cite this article in press as: Kollewe et al., Subunit composition, molecular environment, and activation of native TRPC channels encoded by their *interactomes*, Neuron (2022), https://doi.org/10.1016/j.neuron.2022.09.029

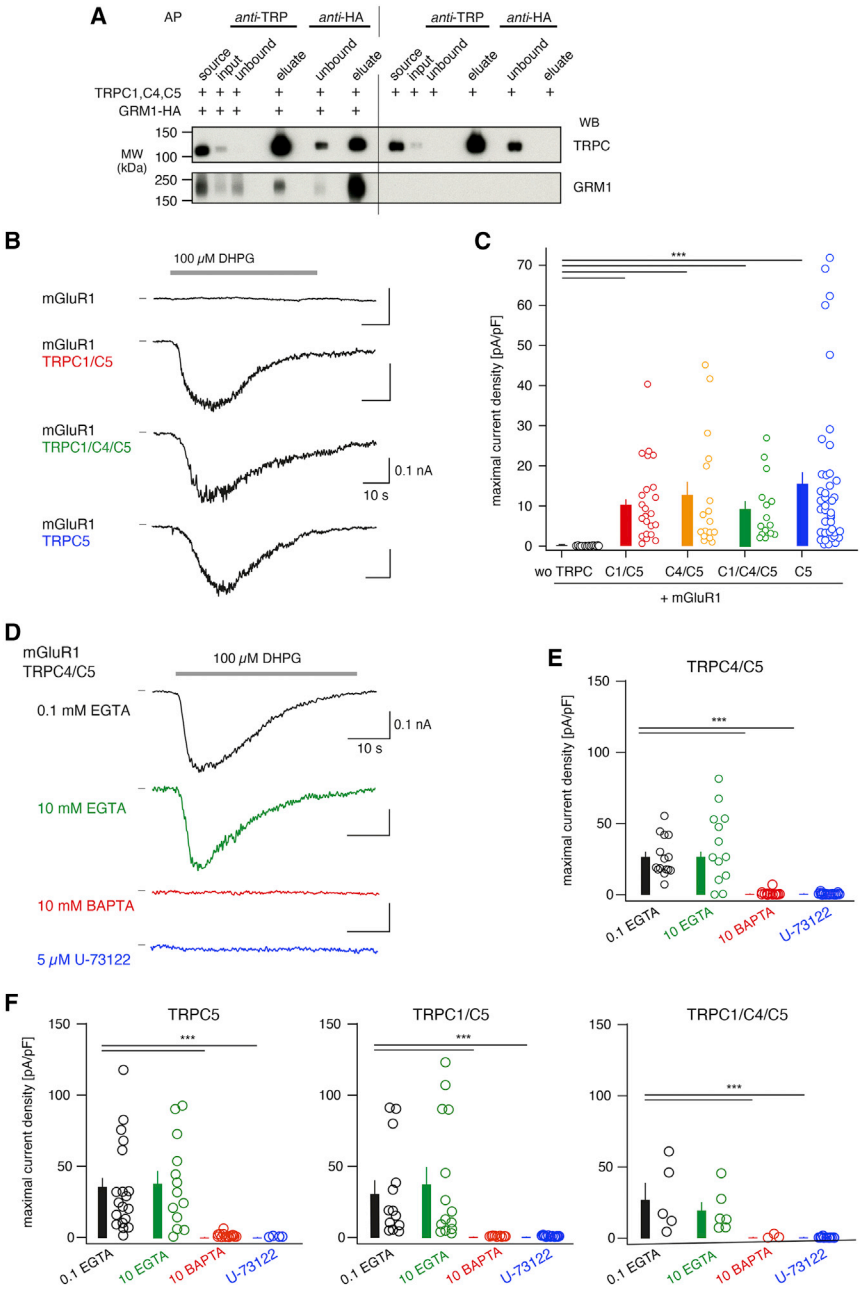

Figure 4. Assembly and operation of TRPC1/C4/C5-mGluR1 complexes in culture cells

(A) APs with *anti*-TRPC4/C5 (4/5C) or *anti*-HA from HEK293T cells transiently transfected with the indicated proteins and Western probed with *anti-TRPC4/C5* (4/5E) (top panel) or *anti-HA* (bottom panel). Molecular weight is indicated on the right. Note robust and specific co-purification of TRPC and mGluR1 in both *anti-HA* and *anti-TRPC* APs.

(B) Representative current traces recorded in HEK293T cells (co)-expressing the indicated proteins in response to the indicated application of DHPG (100 μM). Current and time scaling as indicated.

(C) Plot summarizing maximal current density determined from experiments as in (B). Bars indicate mean ± SEM of the indicated individual experiments given as dots (to the right of all bars); horizontal bars statistical significance at $p < 0.001$ (indicated by three asterisks) determined by non-parametric Mann-Whitney U-test.

(D) Representative DHPG-triggered current traces determined in cells expressing mGluR1-TRPC4/C5 complexes without (0.1 mM EGTA, control, black trace) or with 10 mM EGTA (green trace) or BAPTA (blue trace) in the recording pipette or in cells preincubated with the PLC inhibitor U-73122 (blue trace).

(E) Bars summarizing the experiments in (D). Data are mean ± SEM of the indicated individual experiments given as dots; horizontal bars indicate statistical significance at $p < 0.001$, Mann-Whitney U-test.

(F) Bar graphs as in (E) from experiments with TRPC channels of the indicated subunit composition.

emphasized that the overall abundance of TRPC proteins in the brain is rather low, with amounts more than 500-fold less than those determined for AMPA-type glutamate receptors (Kollewe et al., 2021), metabotropic GABA ($GABA_B$) receptors (Schwenk et al., 2016), or Ca^{2+}-pumps of the plasma membrane (Schmidt et al., 2017). Consequently, analysis of the peripheral subunits of the TRPC assemblies is challenging and strongly depended on some key features of our proteomic approach: (1) application of multiple ABs with distinct epitopes on the target compensating the pitfalls of individual ABs, (2) unbiased and quantitative analysis of all proteins in AP eluates, (3) sensitivity and dynamic range of our MS analysis extending over a linear range of up to four orders of magnitude, (4) use of stringent negative controls provided by single and multiple target knockouts, and (5) application of the consistency criterion diminishing the influence of false assignments due to peculiarities of binding properties and background of individual ABs. For TRPCs 1, 4, 5, the combination of these features promoted determination of a comprehensive interactome comprising 15 constituents of TM and soluble proteins (Figure 3; Table 1) whose co-assembly in various combinations explains the high-molecular-weight appearance of native TRPC1/C4/C5 channel complexes (Figures 1C and S5). The functional significance of these co-assemblies has been unveiled here for mGluR1 (Figures 4 and 5, see below) but still remains open for the other interactome constituents that have not been related to TRP channels before, except for INAM2, a reported modulator of TRP channel function in *Drosophila melanogaster* (Chen and Montell, 2020; Cheng and Nash, 2007; Li et al., 1999; Rosenzweig et al., 2008). Similarly, unraveling the significance of the interactors determined for TRPCs 6 and 7 with the

Please cite this article in press as: Kollewe et al., Subunit composition, molecular environment, and activation of native TRPC channels encoded by their *interactomes*, Neuron (2022), https://doi.org/10.1016/j.neuron.2022.09.029

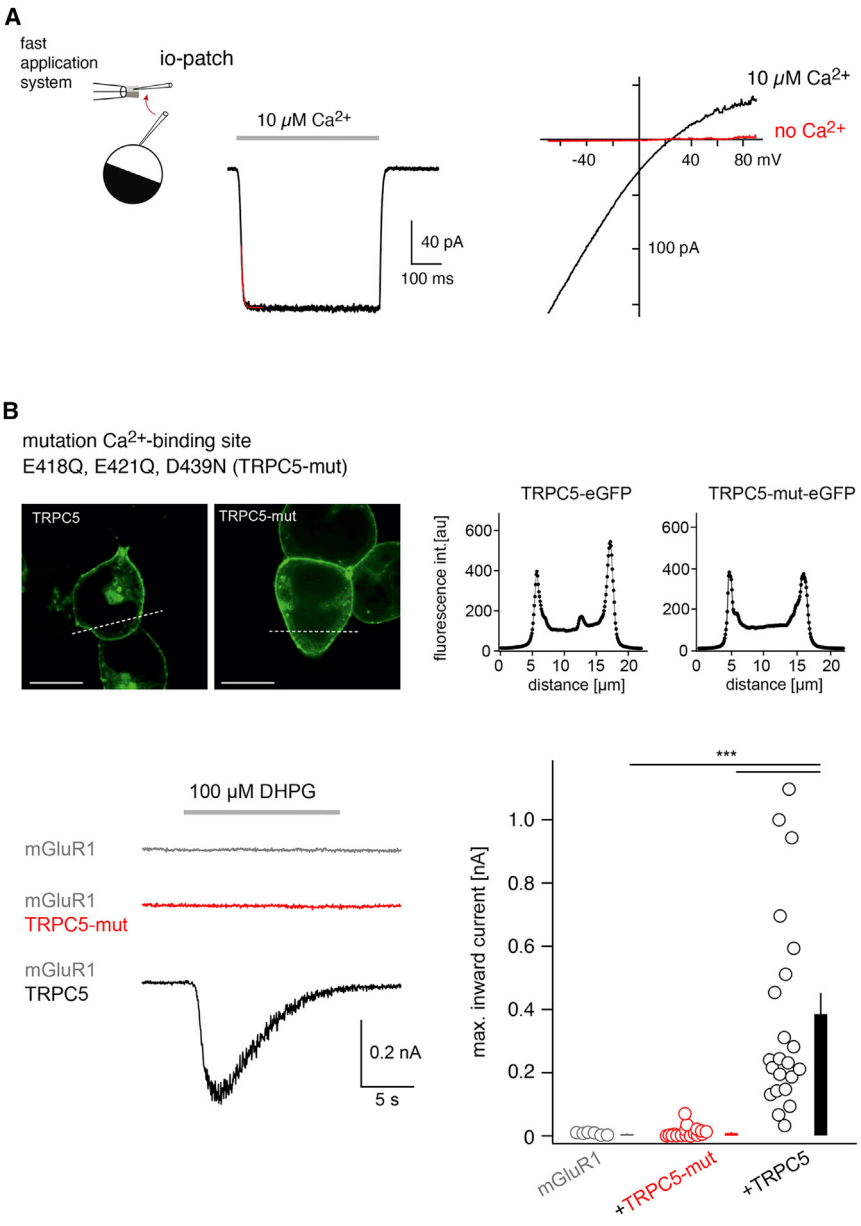

Figure 5. Gating of TRPC channels by direct Ca^{2+}-binding

(A) Representative current responses recorded in giant inside-out patches from TRPC4-expressing Xenopus oocytes either upon fast application (left panel, membrane potential −70 mV) or in the continuous presence (right panel, voltage ramped from −70 to 90 mV in 0.5 s) of 10 μM Ca^{2+} applied to the cytoplasmic side of the membrane. Note that no currents are observed in the absence of Ca^{2+}. Red line on the fast-application response is fit of an exponential function to the rising phase of the current with a time constant of 5.1 ms.

(B) Upper panel: confocal images of HEK293 cells expressing either TRPC5 WT or TRPC5 mutant channels with a triple residue exchange in the Ca^{2+}-binding site (E418Q, E421Q, D439N; TRPC5-mut). Scale bars, 10 μm. Note that both TRPC5 proteins exhibit robust expression in the plasma membrane evidenced by the line scans given on the right. Lower left panel: representative current traces measured in HEK293 cells co-expressing the indicated proteins in response to 100 μM DHPG. Lower right panel: bar graph as in Figure 4 summarizing maximal inward currents determined in experiments as on the left. Data are mean ± SEM of the indicated individual experiments given as dots; horizontal bars indicate statistical significance at $p < 0.001$, Mann-Whitney U-test.

same stringency as used for TRPC1/C4/C5 (Figure 3; Table S3) requires further experimental work.

Finally, it should be noted that our proteomic approach failed to verify most of the previously reported interaction partners of the TRPC proteins despite the sensitivity and extended dynamic range of our MS analyses and the careful application of our evaluation criteria. As another note of caution, it should be mentioned that several of the commercial *anti-TRPC* ABs tested for this work either lacked target-specificity or efficiency of target binding.

Formation of hetero-tetramers with distinct stoichiometry

Quantitative analysis of the pore architecture by serial APs showed that (1) almost all TRPC1, C4, C5 proteins in the brain of wild-type mice are assembled as hetero-tetramers, (2) all of these heteromers contain one TRPC1 subunit, and (3) the only possible TRPC1-free configuration could not be detected (Figures 1 and 2). All of these observations come as a surprise since in heterologous (co)-expressions both, TRPC4 and TRPC5 proteins, are well able to form functional channels of both homomeric and heteromeric configuration(s) (Figure 4B); in contrast, TRPC1 alone failed to provide functional channel activity under the same experimental conditions (Kim et al., 2014; Ko et al., 2019; Storch et al., 2012).

At present, the advantage(s) of the observed hetero-multimer formation is unclear, as is the requirement for the TRPC1 subunit therein. Nonetheless, it appears obvious that TRPC1 works as a "stabilizing factor" that either maintains the other two subunits in heteromeric configurations and/or protects heteromers from degradation. Both of these actions may occur during channel assembly in the ER, trafficking, endosomal retrieval, or processing at the plasma membrane. In either case, TRPC1 may not be expected to act on its own but rather through TRPC1-specific constituents of the interactome such as LASP1 or INAM2 (Figure 3; Table 1). Although such hypotheses require further experimental work, it may well be concluded that the pore-focused analyses, as mostly applied to date, should be extended toward the constituents of the identified interactome(s) in order to understand the TRPC action(s) under native cellular conditions as has been

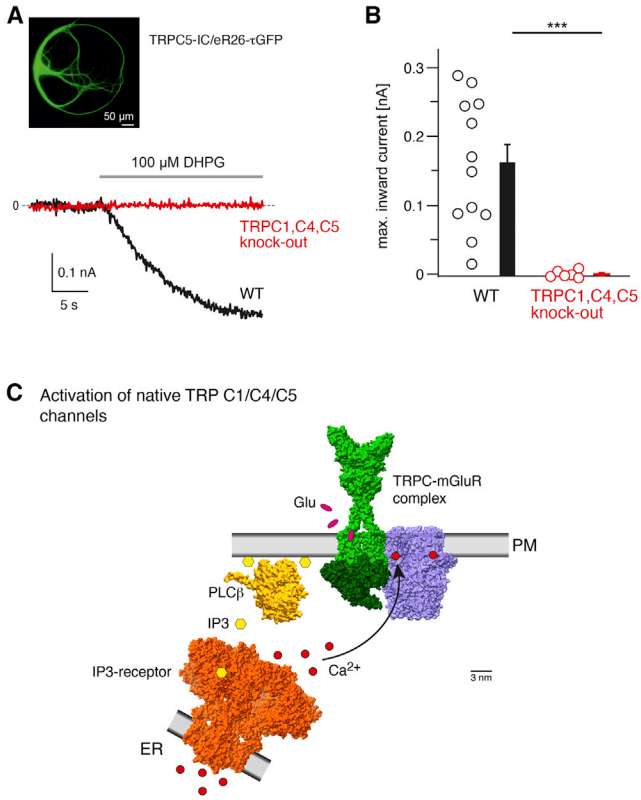

Figure 6. TRPC1/C4/C5-mGluR1 complexes in hippocampal neurons

(A) Representative inward currents recorded in response to DHPG (100 μM) in autaptic cultures of hippocampal neurons (inset, epifluorescence image of an autaptic hippocampal TRPC5-IC/eR26-τGFP neuron where τGFP fluorescence reports endogenous TRPC5 expression, scale bars, 50 μm) from WT (trace in black) and TRPC1, C4, C5 triple-knockout (trace in red). Current and time scaling as indicated; DHPG-solution contained TTX (1 μM), DNQX (25 μM), picrotoxin (30 μM), and D-AP5 (10 μM) to inhibit synaptic transmission.

(B) Bar graph summarizing amplitudes of currents recorded in (A). Bars indicate mean ± SEM of the indicated individual experiments given as dots, and horizontal bar indicates statistical significance at $p < 0.001$, Mann-Whitney U test.

(C) Scheme illustrating operation of the newly identified TRPC1/C4/C5-mGluR complex in the cellular context. 3D structures were taken from the PDB database (PDB: 7B0J [TRPC4, blue], 6N51 [mGluR5, light green], 3SN6 [Gs-protein, dark green], 3OHM [PLCβ3, yellow], and 6UQK [IP_3 receptor, orange]).

demonstrated for ionotropic AMPA-receptors (Boudkkazi et al., 2014; Brechet et al., 2017; Schwenk et al., 2019; Schwenk et al., 2009, 2012) and other types of membrane proteins (Dinamarca et al., 2019; Kise et al., 2021; Korthals et al., 2017; Li et al., 2017; Marionneau et al., 2009; Martin et al., 2019; Schmidt et al., 2017; Schwenk et al., 2010, 2016; Turecek et al., 2014; Zhao and MacKinnon, 2021; Zheng et al., 2019). Moreover, it might be worthwhile to use the approach of serial APs with thorough MS-based protein quantification as introduced here (Figure 2) to resolve the subunit composition of other membrane protein complexes in native tissue.

Significance of TRPC-mGluR complexes

Our proteomic work unveiled direct interaction of TRPC1/C4/C5 with the metabotropic receptor mGluR1, a finding that provides immediate insight into the glutamate-induced activation described for TRPCs in various types of central nervous system (CNS) neurons (Dong et al., 2009; El-Hassar et al., 2011; Gee et al., 2003; Kim et al., 2003; Zhang et al., 2001; Zheng and Phelan, 2014).

In this sense, the identified TRPC1/C4/C5-mGluR1 complex is the centerpiece of a signaling module that is switched on by agonist binding to the GPCR moiety of the complex and provides the depolarizing cation current mediated by the complex' channel moiety as an output (Figure 6C). Both ends of this module are functionally linked by means of the "classical" mGluR1-pathway that uses PLCβ to generate IP_3 and trigger Ca^{2+}-outward currents from the ER via the IP_3-receptor. The resulting increase in intracellular Ca^{2+} finally activates the TRPC channels that are operated here as Ca^{2+}-activated cation channels (Figures 4, 5, and 6).

Conceptually, TRPC1/C4/C5-mGluR1 complexes are different from GPCR-channel complexes where receptor activation is directly converted into channel modulation via the receptor-attached Gβγ-dimer, as established in complexes built from $GABA_B$ receptors and Cav2.2 voltage-gated Ca^{2+}-channels (Schwenk et al., 2016). While in these complexes, the channel moiety acts as the "primary effector" of the GPCR, TRPC1/C4/C5 channels rather act as "secondary effectors" of the co-assembled mGluR1 receptor. In fact, the well-established "primary effector" of mGluR1 is used as a coupling device which, under cellular conditions, may also be a constituent of TRPC1/C4/C5-mGluR1 complexes, but was missed by our proteomic approach due to susceptibility of respective interaction(s) to detergent treatment. On the other hand, it should be noted that TRPC-activation via PLC-coupling receptors may not require physical association with the TRPC channels, as long as the triggered increase in intracellular Ca^{2+} concentration is sufficiently high (in the low micromolar range) to activate the TRPC channels. Similarly Ca^{2+}-activated BK channels are highly reliably activated by co-assembled Cav2.1 channels, although some activation was observed with non-associated Cav2.3 channels due to their robust expression (Berkefeld and Fakler, 2013; Berkefeld et al., 2006).

Nonetheless, TRPC1/C4/C5-mGluR1 complexes represent the evolutionary solution to glutamate-triggered activation of TRPC channels, and the following reasons may be envisaged as underlying advantages. First, complex formation should increase reliability of its operation and respective signaling. Second, GPCR signaling could be restricted to local spatial domains by complex formation (as evidenced by the differential BAPTA effect; Figure 4), and third, it may accelerate signal transduction (Figure 6A). Whether these ideas are realized in the context of neurons and other types of cell and whether assembly of GPCRs with secondary effectors represents a more broadly used principle in GPCR signaling may be clarified by future work. In any case, the presented work provides a first insight into the molecular orchestration of TRPC channels in the brain and sets the stage for future functional studies of these channels in the CNS.

STAR★METHODS

Detailed methods are provided in the online version of this paper and include the following:

- KEY RESOURCES TABLE
- RESOURCE AVAILABILITY
  - Lead contact
  - Materials availability
  - Data and code availability
- EXPERIMENTAL MODEL AND SUBJECT DETAILS
  - Animals
  - Cell lines
  - Primary cells
- METHOD DETAILS
  - Antibodies
  - Molecular biology
  - Generation of TRPC1-IRES-Cre and TRPC4-IRES-Cre mouse strains
  - Immunofluorescence staining of mouse brain sections
  - Biochemistry
  - Mass spectrometry
  - Quantitative evaluation
  - Electrophysiology
- QUANTIFICATION AND STATISTICAL ANALYSIS

SUPPLEMENTAL INFORMATION

Supplemental information can be found online at https://doi.org/10.1016/j.neuron.2022.09.029.

ACKNOWLEDGMENTS

We thank J. Schwenk for critical reading of the manuscript and discussions, U. Wissenbach for cDNA cloning, and C. Wesely for generation of antibodies. Funding: this work was supported by grants of the Deutsche Forschungsgemeinschaft (DFG, German Research Foundation) TRR 152 (project-ID 239283807, P01, P02, P07, and P11 to V.F., B.F., Y.S., D.B., and U.B.), SFB 894 (project-ID 157660137, A11 to D.B., A14 to V.F.), SFB 1381 (project-ID 403222702 to B.F.), FA 332/15-1 and 16-1 (to B.F.), and by grants of the Saarland University (Young Investigator and HOMFor2022 to Y.S.).

AUTHOR CONTRIBUTIONS

V.F. and B.F. conceived the project. A.K., A.H., W.B., and U.S. performed experiments related to protein biochemistry and proteomic analyses. Y.S., K.O., D.B., and G.Z. performed electrophysiology and evaluations in culture cell, neuronal cultures, and oocytes, respectively. A.R., P.W., A.W., and U.B. generated transgenic animals. B.F. evaluated data and wrote the manuscript with the support of all authors.

DECLARATION OF INTERESTS

The authors declare no competing interests.

Received: April 26, 2022
Revised: August 15, 2022
Accepted: September 23, 2022
Published: October 17, 2022

REFERENCES

Bai, Y., Yu, X., Chen, H., Horne, D., White, R., Wu, X., Lee, P., Gu, Y., Ghimire-Rijal, S., Lin, D.C., and Huang, X. (2020). Structural basis for pharmacological modulation of the TRPC6 channel. eLife *9*, e53311. https://doi.org/10.7554/eLife.53311.

Bai, Z., Feng, J., Franken, G.A.C., Al'Saadi, N., Cai, N., Yu, A.S., Lou, L., Komiya, Y., Hoenderop, J.G.J., de Baaij, J.H.F., Yue, L., and Runnels, L.W. (2021). CNNM proteins selectively bind to the TRPM7 channel to stimulate divalent cation entry into cells. PLoS Biol. *19*, e3001496. https://doi.org/10.1371/journal.pbio.3001496.

Berkefeld, H., and Fakler, B. (2013). Ligand-gating by Ca^{2+} is rate limiting for physiological operation of BK(Ca) channels. J. Neurosci. *33*, 7358–7367. https://doi.org/10.1523/JNEUROSCI.5443-12.2013.

Berkefeld, H., Sailer, C.A., Bildl, W., Rohde, V., Thumfart, J.O., Eble, S., Klugbauer, N., Reisinger, E., Bischofberger, J., Oliver, D., et al. (2006). BK_{Ca}-Cav channel complexes mediate rapid and localized Ca^{2+}-activated K^+ signaling. Science *314*, 615–620. https://doi.org/10.1126/science.1132915.

Bezzerides, V.J., Ramsey, I.S., Kotecha, S., Greka, A., and Clapham, D.E. (2004). Rapid vesicular translocation and insertion of TRP channels. Nat. Cell Biol. *6*, 709–720. https://doi.org/10.1038/ncb1150.

Bildl, W., Haupt, A., Müller, C.S., Biniossek, M.L., Thumfart, J.O., Hüber, B., Fakler, B., and Schulte, U. (2012). Extending the dynamic range of label-free mass spectrometric quantification of affinity purifications. Mol. Cell. Proteomics *11*. M111.007955. https://doi.org/10.1074/mcp.M111.007955.

Blair, N.T., Carvacho, I., Chaudhuri, D., Clapham, D.E., DeCaen, P., Delling, M., Doerner, J.F., Fan, L., Ha, K., Jordt, S.E., et al. (2021). Transient receptor potential channels (TRP) in GtoPdb v.2021.3. IUPHAR/BPS Guide to Pharmacology CITE *2021*. https://doi.org/10.2218/gtopdb/F78/2021.3.

Blair, N.T., Kaczmarek, J.S., and Clapham, D.E. (2009). Intracellular calcium strongly potentiates agonist-activated TRPC5 channels. J. Gen. Physiol. *133*, 525–546. https://doi.org/10.1085/jgp.200810153.

Boudkkazi, S., Brechet, A., Schwenk, J., and Fakler, B. (2014). Cornichon2 dictates the time course of excitatory transmission at individual hippocampal synapses. Neuron *82*, 848–858. https://doi.org/10.1016/j.neuron.2014.03.031.

Brechet, A., Buchert, R., Schwenk, J., Boudkkazi, S., Zolles, G., Siquier-Pernet, K., Schaber, I., Bildl, W., Saadi, A., Bole-Feysot, C., et al. (2017). AMPA-receptor specific biogenesis complexes control synaptic transmission and intellectual ability. Nat. Commun. *8*, 15910. https://doi.org/10.1038/ncomms15910.

Bröker-Lai, J., Kollewe, A., Schindeldecker, B., Pohle, J., Nguyen Chi, V., Mathar, I., Guzman, R., Schwarz, Y., Lai, A., Weißgerber, P., et al. (2017). Heteromeric channels formed by TRPC1, TRPC4 and TRPC5 define hippocampal synaptic transmission and working memory. EMBO J. *36*, 2770–2789. https://doi.org/10.15252/embj.201696369.

Camacho Londoño, J.E., Tian, Q., Hammer, K., Schröder, L., Camacho Londoño, J., Reil, J.C., He, T., Oberhofer, M., Mannebach, S., Mathar, I., et al. (2015). A background Ca^{2+} entry pathway mediated by TRPC1/TRPC4 is critical for development of pathological cardiac remodelling. Eur. Heart J. *36*, 2257–2266. https://doi.org/10.1093/eurheartj/ehv250.

Cerny, A.C., and Huber, A. (2011). Regulation of TRP signalling by ion channel translocation between cell compartments. Adv. Exp. Med. Biol. *704*, 545–572. https://doi.org/10.1007/978-94-007-0265-3_30.

Chen, X., Lu, M., He, X., Ma, L., Birnbaumer, L., and Liao, Y. (2017). TRPC3/6/7 Knockdown Protects the Brain from Cerebral ischemia Injury via Astrocyte Apoptosis Inhibition and Effects on NF-small ka, CyrillicB Translocation. Mol. Neurobiol. *54*, 7555–7566. https://doi.org/10.1007/s12035-016-0227-2.

Chen, Z., and Montell, C. (2020). A family of auxiliary subunits of the TRP cation channel encoded by the complex inaF locus. Genetics *215*, 713–728.

Cheng, Y., and Nash, H.A. (2007). Drosophila TRP channels require a protein with a distinctive motif encoded by the inaF locus. Proc. Natl. Acad. Sci. USA *104*, 17730–17734. https://doi.org/10.1073/pnas.0708368104.

Chung, Y.H., Sun Ahn, H., Kim, D., Hoon Shin, D., Su Kim, S., Yong Kim, K., Bok Lee, W., and Ik Cha, C. (2006). Immunohistochemical study on the distribution of TRPC channels in the rat hippocampus. Brain Res. *1085*, 132–137. https://doi.org/10.1016/j.brainres.2006.02.087.

Dietrich, A., Kalwa, H., Storch, U., Mederos y Schnitzler, M., Salanova, B., Pinkenburg, O., Dubrovska, G., Essin, K., Gollasch, M., Birnbaumer, L., and Gudermann, T. (2007). Pressure-induced and store-operated cation influx in vascular smooth muscle cells is independent of TRPC1. Pflugers Arch. *455*, 465–477. https://doi.org/10.1007/s00424-007-0314-3.

Dietrich, A., Mederos, Y.S.M., Gollasch, M., Gross, V., Storch, U., Dubrovska, G., Obst, M., Yildirim, E., Salanova, B., Kalwa, H., et al. (2005). Increased vascular smooth muscle contractility in TRPC6-/- mice. Mol. Cell. Biol. *25*, 6980–6989. https://doi.org/10.1128/MCB.25.16.6980-6989.2005.

Dinamarca, M.C., Raveh, A., Schneider, A., Fritzius, T., Früh, S., Rem, P.D., Stawarski, M., Lalanne, T., Turecek, R., Choo, M., et al. (2019). Complex formation of APP with $GABA_B$ receptors links axonal trafficking to amyloidogenic processing. Nat. Commun. *10*, 1331. https://doi.org/10.1038/s41467-019-09164-3.

Dong, H.W., Hayar, A., Callaway, J., Yang, X.H., Nai, Q., and Ennis, M. (2009). Group I mGluR activation enhances Ca^{2+}-dependent nonselective cation currents and rhythmic bursting in main olfactory bulb external tufted cells. J. Neurosci. *29*, 11943–11953. https://doi.org/10.1523/JNEUROSCI.0206-09.2009.

Duan, J., Li, J., Chen, G.L., Ge, Y., Liu, J., Xie, K., Peng, X., Zhou, W., Zhong, J., Zhang, Y., et al. (2019). Cryo-EM structure of TRPC5 at 2.8-A resolution reveals unique and conserved structural elements essential for channel function. Sci. Adv. *5*, eaaw7935. https://doi.org/10.1126/sciadv.aaw7935.

Duan, J., Li, J., Zeng, B., Chen, G.-L., Peng, X., Zhang, Y., Wang, J., Clapham, D.E., Li, Z., and Zhang, J. (2018). Structure of the mouse TRPC4 ion channel. Nat. Commun. *9*, 3102. https://doi.org/10.1038/s41467-018-05247-9.

Dymecki, S.M. (1996). Flp recombinase promotes site-specific DNA recombination in embryonic stem cells and transgenic mice. Proc. Natl. Acad. Sci. USA *93*, 6191–6196. https://doi.org/10.1073/pnas.93.12.6191.

El-Hassar, L., Hagenston, A.M., D'Angelo, L.B., and Yeckel, M.F. (2011). Metabotropic glutamate receptors regulate hippocampal CA1 pyramidal neuron excitability via Ca^{2+} wave-dependent activation of SK and TRPC channels. J. Physiol. *589*, 3211–3229. https://doi.org/10.1113/jphysiol.2011.209783.

Fakler, B., and Adelman, J.P. (2008). Control of K_{Ca} channels by calcium Nano/microdomains. Neuron *59*, 873–881. https://doi.org/10.1016/j.neuron.2008.09.001.

Flockerzi, V., Jung, C., Aberle, T., Meissner, M., Freichel, M., Philipp, S.E., Nastainczyk, W., Maurer, P., and Zimmermann, R. (2005). Specific detection and semi-quantitative analysis of TRPC4 protein expression by antibodies. Pflugers Arch. *451*, 81–86. https://doi.org/10.1007/s00424-005-1443-1.

Fogel, B.L., Hanson, S.M., and Becker, E.B. (2015). Do mutations in the murine ataxia gene TRPC3 cause cerebellar ataxia in humans? Mov. Disord. *30*, 284–286. https://doi.org/10.1002/mds.26096.

Freichel, M., Suh, S.H., Pfeifer, A., Schweig, U., Trost, C., Weissgerber, P., Biel, M., Philipp, S., Freise, D., Droogmans, G., et al. (2001). Lack of an endothelial store-operated Ca2+ current impairs agonist-dependent vasorelaxation in TRP4-/- mice. Nat. Cell Biol. *3*, 121–127. https://doi.org/10.1038/35055019.

Freichel, M., Vennekens, R., Olausson, J., Stolz, S., Philipp, S.E., Weissgerber, P., and Flockerzi, V. (2005). Functional role of TRPC proteins in native systems: implications from knockout and knock-down studies. J. Physiol. *567*, 59–66. https://doi.org/10.1113/jphysiol.2005.092999.

Gaudet, R. (2008). TRP channels entering the structural era. J. Physiol. *586*, 3565–3575. https://doi.org/10.1113/jphysiol.2008.155812.

Gee, C.E., Benquet, P., and Gerber, U. (2003). Group I metabotropic glutamate receptors activate a calcium-sensitive transient receptor potential-like conductance in rat hippocampus. J. Physiol. *546*, 655–664. https://doi.org/10.1113/jphysiol.2002.032961.

Gross, S.A., Guzmán, G.A., Wissenbach, U., Philipp, S.E., Zhu, M.X., Bruns, D., and Cavalié, A. (2009). TRPC5 is a Ca^{2+}-activated channel functionally coupled to Ca^{2+}-selective ion channels. J. Biol. Chem. *284*, 34423–34432. https://doi.org/10.1074/jbc.M109.018192.

Hartmann, J., Dragicevic, E., Adelsberger, H., Henning, H.A., Sumser, M., Abramowitz, J., Blum, R., Dietrich, A., Freichel, M., Flockerzi, V., et al. (2008). TRPC3 channels are required for synaptic transmission and motor coordination. Neuron *59*, 392–398. https://doi.org/10.1016/j.neuron.2008.06.009.

Heukeshoven, J., and Dernick, R. (1988). Improved silver staining procedure for fast staining in PhastSystem Development Unit. I. Staining of sodium dodecyl sulfate gels. Electrophoresis *9*, 28–32. https://doi.org/10.1002/elps.1150090106.

Hirnet, D., Olausson, J., Fecher-Trost, C., Bödding, M., Nastainczyk, W., Wissenbach, U., Flockerzi, V., and Freichel, M. (2003). The TRPV6 gene, cDNA and protein. Cell Calcium *33*, 509–518. https://doi.org/10.1016/s0143-4160(03)00066-6.

Hofmann, T., Obukhov, A.G., Schaefer, M., Harteneck, C., Gudermann, T., and Schultz, G. (1999). Direct activation of human TRPC6 and TRPC3 channels by diacylglycerol. Nature *397*, 259–263. https://doi.org/10.1038/16711.

Huang, G.N., Zeng, W., Kim, J.Y., Yuan, J.P., Han, L., Muallem, S., and Worley, P.F. (2006). STIM1 carboxyl-terminus activates native SOC, I(crac) and TRPC1 channels. Nat. Cell Biol. *8*, 1003–1010. https://doi.org/10.1038/ncb1454.

Jeon, J., Bu, F., Sun, G., Tian, J.B., Ting, S.M., Li, J., Aronowski, J., Birnbaumer, L., Freichel, M., and Zhu, M.X. (2020). Contribution of TRPC channels in neuronal excitotoxicity associated With neurodegenerative disease and ischemic stroke. Front. Cell Dev. Biol. *8*, 618663. https://doi.org/10.3389/fcell.2020.618663.

Kim, J., Kwak, M., Jeon, J.-P., Myeong, J., Wie, J., Hong, C., Kim, S.-Y., Jeon, J.-H., Kim, H.J., and So, I. (2014). Isoform- and receptor-specific channel property of canonical transient receptor potential (TRPC)1/4 channels. Pflugers Arch. *466*, 491–504. https://doi.org/10.1007/s00424-013-1332-y.

Kim, S.J., Kim, Y.S., Yuan, J.P., Petralia, R.S., Worley, P.F., and Linden, D.J. (2003). Activation of the TRPC1 cation channel by metabotropic glutamate receptor mGluR1. Nature *426*, 285–291. https://doi.org/10.1038/nature02162.

Kirtley, P.R., Sooch, G.S., White, F.A., and Obukhov, A.G. (2021). Transient receptor potential canonical channels in health and disease: A 2020 update. Cells *10*, 496. https://doi.org/10.3390/cells10030496.

Kise, Y., Kasuya, G., Okamoto, H.H., Yamanouchi, D., Kobayashi, K., Kusakizako, T., Nishizawa, T., Nakajo, K., and Nureki, O. (2021). Structural basis of gating modulation of Kv4 channel complexes. Nature *599*, 158–164. https://doi.org/10.1038/s41586-021-03935-z.

Kiselyov, K., Mignery, G.A., Zhu, M.X., and Muallem, S. (1999). The N-terminal domain of the IP3 receptor gates store-operated hTrp3 channels. Mol. Cell *4*, 423–429. https://doi.org/10.1016/s1097-2765(00)80344-5.

Ko, J., Myeong, J., Shin, Y.-C., and So, I. (2019). Differential PI(4,5)P2 sensitivities of TRPC4, C5 homomeric and TRPC1/4, C1/5 heteromeric channels. Sci. Rep. *9*, 1849. https://doi.org/10.1038/s41598-018-38443-0.

Ko, J., Myeong, J., Yang, D., and So, I. (2017). Calcium permeability of transient receptor potential canonical (TRPC) 4 channels measured by TRPC4-GCaMP6s. Korean J. Physiol. Pharmacol. *21*, 133–140. https://doi.org/10.4196/kjpp.2017.21.1.133.

Kollewe, A., Chubanov, V., Tseung, F.T., Correia, L., Schmidt, E., Rössig, A., Zierler, S., Haupt, A., Müller, C.S., Bildl, W., et al. (2021). The molecular appearance of native TRPM7 channel complexes identified by high-resolution proteomics. eLife *10*, e68544. https://doi.org/10.7554/eLife.68544.

Korthals, M., Langnaese, K., Smalla, K.H., Kähne, T., Herrera-Molina, R., Handschuh, J., Lehmann, A.C., Mamula, D., Naumann, M., Seidenbecher, C., et al. (2017). A complex of Neuroplastin and Plasma Membrane Ca^{2+} ATPase controls T cell activation. Sci. Rep. *7*, 8358. https://doi.org/10.1038/s41598-017-08519-4.

Lee, K.P., Choi, S., Hong, J.H., Ahuja, M., Graham, S., Ma, R., So, I., Shin, D.M., Muallem, S., and Yuan, J.P. (2014). Molecular determinants mediating gating of transient receptor potential canonical (TRPC) channels by stromal interaction molecule 1 (STIM1). J. Biol. Chem. *289*, 6372–6382. https://doi.org/10.1074/jbc.M113.546556.

Lee, K.P., Yuan, J.P., So, I., Worley, P.F., and Muallem, S. (2010). STIM1-dependent and STIM1-independent function of transient receptor potential canonical (TRPC) channels tunes their store-operated mode. J. Biol. Chem. *285*, 38666–38673. https://doi.org/10.1074/jbc.M110.155036.

Li, C., Geng, C., Leung, H.T., Hong, Y.S., Strong, L.L., Schneuwly, S., and Pak, W.L. (1999). INAF, a protein required for transient receptor potential Ca^{2+} channel function. Proc. Natl. Acad. Sci. USA *96*, 13474–13479. https://doi.org/10.1073/pnas.96.23.13474.

Li, N., Wu, J.X., Ding, D., Cheng, J., Gao, N., and Chen, L. (2017). Structure of a pancreatic ATP-sensitive potassium channel. Cell *168*, 101–110.e10. https://doi.org/10.1016/j.cell.2016.12.028.

Lintschinger, B., Balzer-Geldsetzer, M., Baskaran, T., Graier, W.F., Romanin, C., Zhu, M.X., and Groschner, K. (2000). Coassembly of Trp1 and Trp3 proteins generates diacylglycerol- and Ca^{2+}-sensitive cation channels. J. Biol. Chem. *275*, 27799–27805. https://doi.org/10.1074/jbc.M002705200.

Marionneau, C., LeDuc, R.D., Rohrs, H.W., Link, A.J., Townsend, R.R., and Nerbonne, J.M. (2009). Proteomic analyses of native brain Kv4.2 channel complexes. Channels (Austin) *3*, 284–294. https://doi.org/10.4161/chan.3.4.9553.

Martin, G.M., Sung, M.W., Yang, Z., Innes, L.M., Kandasamy, B., David, L.L., Yoshioka, C., and Shyng, S.L. (2019). Mechanism of pharmacochaperoning in a mammalian KATP channel revealed by cryo-EM. eLife *8*, e46417. https://doi.org/10.7554/eLife.46417.

Maruyama, Y., Nakanishi, Y., Walsh, E.J., Wilson, D.P., Welsh, D.G., and Cole, W.C. (2006). Heteromultimeric TRPC6-TRPC7 channels contribute to arginine vasopressin-induced cation current of A7r5 vascular smooth muscle cells. Circ. Res. *98*, 1520–1527. https://doi.org/10.1161/01.RES.0000226495.34949.28.

Miller, M., Shi, J., Zhu, Y., Kustov, M., Tian, J.B., Stevens, A., Wu, M., Xu, J., Long, S., Yang, P., et al. (2011). Identification of ML204, a novel potent antagonist that selectively modulates native TRPC4/C5 ion channels. J. Biol. Chem. *286*, 33436–33446. https://doi.org/10.1074/jbc.M111.274167.

Montell, C. (2005). The TRP superfamily of cation channels. Sci. STKE *2005*, re3. https://doi.org/10.1126/stke.2722005re3.

Müller, C.S., Haupt, A., Bildl, W., Schindler, J., Knaus, H.G., Meissner, M., Rammner, B., Striessnig, J., Flockerzi, V., Fakler, B., and Schulte, U. (2010). Quantitative proteomics of the Cav2 channel nano-environments in the mammalian brain. Proc. Natl. Acad. Sci. USA *107*, 14950–14957. https://doi.org/10.1073/pnas.1005940107.

Myeong, J., Ko, J., Hong, C., Yang, D., Lee, K.P., Jeon, J.-H., and So, I. (2016). The interaction domains of transient receptor potential canonical (TRPC)1/4 and TRPC1/5 heteromultimeric channels. Biochem. Biophys. Res. Commun. *474*, 476–481. https://doi.org/10.1016/j.bbrc.2016.04.138.

Perez-Leighton, C.E., Schmidt, T.M., Abramowitz, J., Birnbaumer, L., and Kofuji, P. (2011). Intrinsic phototransduction persists in melanopsin-expressing ganglion cells lacking diacylglycerol-sensitive TRPC subunits. Eur. J. Neurosci. *33*, 856–867. https://doi.org/10.1111/j.1460-9568.2010.07583.x.

Philipp, S., Trost, C., Warnat, J., Rautmann, J., Himmerkus, N., Schroth, G., Kretz, O., Nastainczyk, W., Cavalie, A., Hoth, M., and Flockerzi, V. (2000). TRP4 (CCE1) protein is part of native calcium release-activated Ca2+-like channels in adrenal cells. J. Biol. Chem. *275*, 23965–23972. https://doi.org/10.1074/jbc.M003408200.

Riccio, A., Medhurst, A.D., Mattei, C., Kelsell, R.E., Calver, A.R., Randall, A.D., Benham, C.D., and Pangalos, M.N. (2002). mRNA distribution analysis of human TRPC family in CNS and peripheral tissues. Brain Res. Mol. Brain Res. *109*, 95–104. https://doi.org/10.1016/s0169-328x(02)00527-2.

Rosenzweig, M., Kang, K., and Garrity, P.A. (2008). Distinct TRP channels are required for warm and cool avoidance in *Drosophila melanogaster*. Proc. Natl. Acad. Sci. USA *105*, 14668–14673. https://doi.org/10.1073/pnas.0805041105.

Schmidt, N., Kollewe, A., Constantin, C.E., Henrich, S., Ritzau-Jost, A., Bildl, W., Saalbach, A., Hallermann, S., Kulik, A., Fakler, B., and Schulte, U. (2017). Neuroplastin and basigin are essential auxiliary subunits of plasma membrane Ca^{2+}-ATPases and key regulators of Ca^{2+} clearance. Neuron *96*, 827–838.e9. https://doi.org/10.1016/j.neuron.2017.09.038.

Schneider, C.A., Rasband, W.S., and Eliceiri, K.W. (2012). NIH Image to ImageJ: 25 years of Image Analysis. Nat. Methods *9*, 671–675. https://doi.org/10.1038/nmeth.2089.

Schwarz, Y., Oleinikov, K., Schindeldecker, B., Wyatt, A., Weißgerber, P., Flockerzi, V., Boehm, U., Freichel, M., and Bruns, D. (2019). TRPC channels regulate Ca2+-signaling and short-term plasticity of fast glutamatergic synapses. PLoS Biol. *17*, e3000445. https://doi.org/10.1371/journal.pbio.3000445.

Schwenk, J., Boudkkazi, S., Kocylowski, M.K., Brechet, A., Zolles, G., Bus, T., Costa, K., Kollewe, A., Jordan, J., Bank, J., et al. (2019). An ER assembly line of AMPA-receptors controls excitatory neurotransmission and its plasticity. Neuron *104*, 680–692.e9. https://doi.org/10.1016/j.neuron.2019.08.033.

Schwenk, J., Harmel, N., Brechet, A., Zolles, G., Berkefeld, H., Müller, C.S., Bildl, W., Baehrens, D., Hüber, B., Kulik, A., et al. (2012). High-resolution proteomics unravel architecture and molecular diversity of native AMPA receptor complexes. Neuron *74*, 621–633. https://doi.org/10.1016/j.neuron.2012.03.034.

Schwenk, J., Harmel, N., Zolles, G., Bildl, W., Kulik, A., Heimrich, B., Chisaka, O., Jonas, P., Schulte, U., Fakler, B., and Klöcker, N. (2009). Functional proteomics identify cornichon proteins as auxiliary subunits of AMPA receptors. Science *323*, 1313–1319. https://doi.org/10.1126/science.1167852.

Schwenk, J., Metz, M., Zolles, G., Turecek, R., Fritzius, T., Bildl, W., Tarusawa, E., Kulik, A., Unger, A., Ivankova, K., et al. (2010). Native $GABA_B$ receptors are heteromultimers with a family of auxiliary subunits. Nature *465*, 231–235. https://doi.org/10.1038/nature08964.

Schwenk, J., Pérez-Garci, E., Schneider, A., Kollewe, A., Gauthier-Kemper, A., Fritzius, T., Raveh, A., Dinamarca, M.C., Hanuschkin, A., Bildl, W., et al. (2016). Modular composition and dynamics of native $GABA_B$ receptors identified by high-resolution proteomics. Nat. Neurosci. *19*, 233–242. https://doi.org/10.1038/nn.4198.

Selvaraj, S., Sun, Y., and Singh, B.B. (2010). TRPC channels and their implication in neurological diseases. CNS Neurol. Disord. Drug Targets *9*, 94–104. https://doi.org/10.2174/187152710790966650.

Sierra-Valdez, F., Azumaya, C.M., Romero, L.O., Nakagawa, T., and Cordero-Morales, J.F. (2018). Structure-function analyses of the ion channel TRPC3 reveal that its cytoplasmic domain allosterically modulates channel gating. J. Biol. Chem. *293*, 16102–16114. https://doi.org/10.1074/jbc.RA118.005066.

Song, K., Wei, M., Guo, W., Quan, L., Kang, Y., Wu, J.X., and Chen, L. (2021). Structural basis for human TRPC5 channel inhibition by two distinct inhibitors. eLife *10*, e63429. https://doi.org/10.7554/eLife.63429.

Storch, U., Forst, A.-L., Philipp, M., Gudermann, T., and Mederos y Schnitzler, M. (2012). Transient receptor potential channel 1 (TRPC1) reduces calcium permeability in heteromeric channel complexes. J. Biol. Chem. *287*, 3530–3540. https://doi.org/10.1074/jbc.M111.283218.

Strübing, C., Krapivinsky, G., Krapivinsky, L., and Clapham, D.E. (2001). TRPC1 and TRPC5 form a novel cation channel in mammalian brain. Neuron *29*, 645–655. https://doi.org/10.1016/s0896-6273(01)00240-9.

Tai, C., Hines, D.J., Choi, H.B., and MacVicar, B.A. (2011). Plasma membrane insertion of TRPC5 channels contributes to the cholinergic plateau potential in hippocampal CA1 pyramidal neurons. Hippocampus *21*, 958–967. https://doi.org/10.1002/hipo.20807.

Tang, J., Lin, Y., Zhang, Z., Tikunova, S., Birnbaumer, L., and Zhu, M.X. (2001). Identification of common binding sites for calmodulin and inositol 1,4,5-trisphosphate receptors on the carboxyl termini of trp channels. J. Biol. Chem. *276*, 21303–21310. https://doi.org/10.1074/jbc.M102316200.

Tang, Q., Guo, W., Zheng, L., Wu, J.X., Liu, M., Zhou, X., Zhang, X., and Chen, L. (2018). Structure of the receptor-activated human TRPC6 and TRPC3 ion channels. Cell Res. *28*, 746–755. https://doi.org/10.1038/s41422-018-0038-2.

Tsvilovskyy, V.V., Zholos, A.V., Aberle, T., Philipp, S.E., Dietrich, A., Zhu, M.X., Birnbaumer, L., Freichel, M., and Flockerzi, V. (2009). Deletion of TRPC4 and TRPC6 in mice impairs smooth muscle contraction and intestinal motility

in vivo. Gastroenterology *137*, 1415–1424. https://doi.org/10.1053/j.gastro.2009.06.046.

Turecek, R., Schwenk, J., Fritzius, T., Ivankova, K., Zolles, G., Adelfinger, L., Jacquier, V., Besseyrias, V., Gassmann, M., Schulte, U., et al. (2014). Auxiliary $GABA_B$ receptor subunits uncouple G protein betagamma subunits from effector channels to induce desensitization. Neuron *82*, 1032–1044. https://doi.org/10.1016/j.neuron.2014.04.015.

Venkatachalam, K., and Montell, C. (2007). TRP channels. Annu. Rev. Biochem. *76*, 387–417. https://doi.org/10.1146/annurev.biochem.75.103004.142819.

Venkatachalam, K., Zheng, F., and Gill, D.L. (2003). Regulation of canonical transient receptor potential (TRPC) channel function by diacylglycerol and protein kinase C. J. Biol. Chem. *278*, 29031–29040. https://doi.org/10.1074/jbc.M302751200.

Vinayagam, D., Mager, T., Apelbaum, A., Bothe, A., Merino, F., Hofnagel, O., Gatsogiannis, C., and Raunser, S. (2018). Electron cryo-microscopy structure of the canonical TRPC4 ion channel. eLife *7*, e36615. https://doi.org/10.7554/eLife.36615.

Vinayagam, D., Quentin, D., Yu-Strzelczyk, J., Sitsel, O., Merino, F., Stabrin, M., Hofnagel, O., Yu, M., Ledeboer, M.W., Nagel, G., et al. (2020). Structural basis of TRPC4 regulation by calmodulin and pharmacological agents. eLife *9*, e60603. https://doi.org/10.7554/eLife.60603.

Wang, H., Cheng, X., Tian, J., Xiao, Y., Tian, T., Xu, F., Hong, X., and Zhu, M.X. (2020). TRPC channels: structure, function, regulation and recent advances in small molecular probes. Pharmacol. Ther. *209*, 107497. https://doi.org/10.1016/j.pharmthera.2020.107497.

Wang, Y., Bu, J., Shen, H., Li, H., Wang, Z., and Chen, G. (2017). Targeting transient receptor potential canonical channels for diseases of the nervous system. Curr. Drug Targets *18*, 1460–1465. https://doi.org/10.2174/1389450117666151209120007.

Wen, S., Götze, I.N., Mai, O., Schauer, C., Leinders-Zufall, T., and Boehm, U. (2011). Genetic identification of GnRH receptor neurons: a new model for studying neural circuits underlying reproductive physiology in the mouse brain. Endocrinology *152*, 1515–1526. https://doi.org/10.1210/en.2010-1208.

Wettschureck, N., and Offermanns, S. (2005). Mammalian G proteins and their cell type specific functions. Physiol. Rev. *85*, 1159–1204. https://doi.org/10.1152/physrev.00003.2005.

Wright, D.J., Simmons, K.J., Johnson, R.M., Beech, D.J., Muench, S.P., and Bon, R.S. (2020). Human TRPC5 structures reveal interaction of a xanthine-based TRPC1/4/5 inhibitor with a conserved lipid binding site. Commun. Biol. *3*, 704. https://doi.org/10.1038/s42003-020-01437-8.

Wyatt, A., Wartenberg, P., Candlish, M., Krasteva-Christ, G., Flockerzi, V., and Boehm, U. (2017). Genetic strategies to analyze primary TRP channel-expressing cells in mice. Cell Calcium *67*, 91–104. https://doi.org/10.1016/j.ceca.2017.05.009.

Xue, T., Do, M.T., Riccio, A., Jiang, Z., Hsieh, J., Wang, H.C., Merbs, S.L., Welsbie, D.S., Yoshioka, T., Weissgerber, P., et al. (2011). Melanopsin signalling in mammalian iris and retina. Nature *479*, 67–73. https://doi.org/10.1038/nature10567.

Yuan, J.P., Kim, M.S., Zeng, W., Shin, D.M., Huang, G., Worley, P.F., and Muallem, S. (2009). TRPC channels as STIM1-regulated SOCs. Channels (Austin) *3*, 221–225. https://doi.org/10.4161/chan.3.4.9198.

Zhang, Z., Tang, J., Tikunova, S., Johnson, J.D., Chen, Z., Qin, N., Dietrich, A., Stefani, E., Birnbaumer, L., and Zhu, M.X. (2001). Activation of Trp3 by inositol 1,4,5-trisphosphate receptors through displacement of inhibitory calmodulin from a common binding domain. Proc. Natl. Acad. Sci. USA *98*, 3168–3173. https://doi.org/10.1073/pnas.051632698.

Zhao, C., and MacKinnon, R. (2021). Molecular structure of an open human KATP channel. Proc. Natl. Acad. Sci. USA *118*. e2112267118. https://doi.org/10.1073/pnas.2112267118.

Zheng, F., and Phelan, K.D. (2014). The role of canonical transient receptor potential channels in seizure and excitotoxicity. Cells *3*, 288–303. https://doi.org/10.3390/cells3020288.

Zheng, S., Abreu, N., Levitz, J., and Kruse, A.C. (2019). Structural basis for KCTD-mediated rapid desensitization of GABAB signalling. Nature *567*, 127–131. https://doi.org/10.1038/s41586-019-0990-0.

Please cite this article in press as: Kollewe et al., Subunit composition, molecular environment, and activation of native TRPC channels encoded by their *interactomes*, Neuron (2022), https://doi.org/10.1016/j.neuron.2022.09.029

CellPress

STAR★METHODS

KEY RESOURCES TABLE

REAGENT or RESOURCE	SOURCE	IDENTIFIER
Antibodies		
Rat anti HA	Roche	Cat#11867423001; RRID:AB_390918
Goat anti rabbit HRP	Abcam	Cat#ab7090; RRID:AB_955417
Goat anti rat HRP	Abcam	Cat#ab7095; RRID:AB_955589
Mouse anti TRPC4 (4C)	NeuroMab	Cat#75-119; RRID:AB_2256454
Mouse anti mGluR1a	BD Biosciences	Cat#610965; RRID:AB_398278
Rabbit anti mGluR1	Biomol	Cat#SA610; RRID:AB_10554323
anti TRPC: see Table S1	this paper	N/A
anti INAM2: see Table S1	this paper	N/A
Biological samples		
brain: mouse, C57BL/6N	Charles River	JAX stock#005304
brain: mouse, TRPC1-/-	Bröker-Lai et al., 2017	C57Bl6/N
brain: mouse, TRPC3-/-	Hartmann et al., 2008	C57Bl6/N
brain: mouse, TRPC4-/-	Bröker-Lai et al., 2017	C57Bl6/N
brain: mouse, TRPC5-/-	Bröker-Lai et al., 2017	C57Bl6/N
brain: mouse, TRPC6-/-	Dietrich et al., 2005	C57Bl6/N
brain: mouse, TRPC7-/-	Perez-Leighton et al., 2011	129B6F1
brain: mouse, TRPC3/C6/C7-triple-/-	this paper	129B6F1
brain: mouse: TRPC1/C4/C5-triple -/-	Bröker-Lai et al., 2017	C57Bl6/N
Chemicals, peptides, and recombinant proteins		
ComplexioLyte CL-47	Logopharm GmbH	Cat#CL-47-01
ComplexioLyte CL-91	Logopharm GmbH	Cat#CL-91-01
Trypsin, sequencing grade modified	Promega	Cat#V5111
Tetrodotoxin	Abcam	Cat#ab120055
DNQX	Tocris	Cat#2312
APV	Tocris	Cat#D-140
DHPG	Tocris	Cat#0342/10
Picrotoxin	Abcam	Cat#ab120315
Bicucullin	Sigma	Cat#14340
BAPTA	Fisher, Germany	Cat#10296722
U-73122	Sigma	Cat#U6756
Critical commercial assays		
Bio-Rad Protein Assay	Bio-Rad	Cat#:5000006
Deposited data		
MS-data	this paper	PRIDE data repository ProteomeXchange: PXD036019
Experimental models: Cell lines		
human tsA201	Sigma	Cat#96121229; RRID:CVCL_2737
Hek M2R	Miller et al., 2011	N/A
Hek M2R TRPC5	Miller et al., 2011	N/A
Experimental models: Organisms/strains		
Rat: Wistar	Charles River	Strain code:003
Mouse: C57BL/6N	Charles River	JAX stock#005304; RRID:IMSR_JAX:005304

(*Continued on next page*)

Continued

REAGENT or RESOURCE	SOURCE	IDENTIFIER
Mouse: TRPC1/C4/C5-triple -/-	Bröker-Lai et al., 2017	C57Bl6/N
Mouse: TRPC1 IC eR26τGFP	this paper	C57Bl6/N
Mouse: TRPC4 IC eR26τGFP	this paper	C57BL6/N
Mouse: TRPC5 IC eR26τGFP	Schwarz et al., 2019	C57BL6/N
Mouse: eROSA26-τGFP	Wen et al., 2011	N/A
Mouse: TRPC1-/-	Bröker-Lai et al., 2017	C57Bl6/N
Mouse: TRPC3-/-	Hartmann et al., 2008	C57Bl6/N
Mouse: TRPC4-/-	Bröker-Lai et al., 2017	C57Bl6/N
Mouse: TRPC5-/-	Bröker-Lai et al., 2017	C57Bl6/N
Mouse: TRPC6-/-	Dietrich et al., 2005	C57Bl6/N
Mouse: TRPC7-/-	Perez-Leighton et al., 2011	129B6F1
Mouse: TRPC3/C6/C7-triple -/-	this paper	129B6F1
Oligonucleotides		
Trpc1-IRES-Cre mice genotyping CM-133: 5′-GCGCCAAGATCTGTCAAAATT-3’	this paper	N/A
Trpc1-IRES-Cre mice genotyping CM-135: 5′-GGCTTCTGAGGCGGAAAGA-3’	this paper	N/A
Trpc1-IRES-Cre mice genotyping CM-136: 5′-GCAAGTATGCAAATACAGTCT-3’	this paper	N/A
Trpc1-IRES-Cre mice genotyping CM-145: 5′-CCGTAACCTGGATAGTGAAAC-3’	this paper	N/A
Trpc1-IRES-Cre mice genotyping CM-148: 5′-CCAGCCTCTGAGCCCAGAA-3’	this paper	N/A
Trpc1-IRES-Cre mice genotyping AR-76: 5′-GGATTTGCTTGGCTTTCGGA-3’	this paper	N/A
Trpc1-IRES-Cre mice genotyping AR-79: 5′-GGGCGGAATTCATCGATGAT-3’	this paper	N/A
Trpc4-IRES-Cre mice genotyping WTF: 5’-AGGTGGTGGTGGAAGACACC-3’	this paper	N/A
Trpc4-IRES-Cre mice genotyping WTR: 5’-TTGCCTGCCCAGAGCACTA-3’	this paper	N/A
Trpc4-IRES-Cre mice genotyping NeoremF: 5’-AACTAAACTGGTCGAGCGATGG-3’	this paper	N/A
Recombinant DNA		
pEGFP-N1	NovoPro	Cat#: V012021#
pN1-TRPC1	this paper	NM_011643
pN1-TRPC5	this paper	MGI:109524
pN1-TRPC4	this paper	NM_016984.3
pN1-TRPC5$^{E418Q/E421Q/D439N}$	this paper	N/A
pcDNA3-mouseGrm1a-HA-Tag	this paper	NP_058672.1
pcDNA3-mouseGrm1b-HA-Tag	this paper	NP_001107805.1
pcAGGS-mINAM2-IRES-GFP	this paper	NM_001301269.1
Software and algorithms		
msconvert.exe	ProteoWizard	http://proteowizard.sourceforge.net/
MaxQuant v1.6.3	Max-Planck-Institute of Biochemistry	http://www.maxquant.org
Mascot 2.6.2	Matrix Science, UK	https://www.matrixscience.com/
BELKI software suite	University of Freiburg, Institute of Physiology 2	https://github.com/phys2/belki

(*Continued on next page*)

Continued

REAGENT or RESOURCE	SOURCE	IDENTIFIER
Pulse	Heka, Germany	https://heka.com/downloads/downloads_main.html#down_patchmaster
Igor Pro 5.01	WaveMetrics, USA	https://www.wavemetrics.com/
VisiView	Visitron, Germany	https://www.visitron.de/index.html
GraphPad Prism 9.0	GraphPad, USA	https://www.graphstats.net/graphpad-prism
SigmaPlot 13.0	Systat, USA	https://systatsoftware.com/
ImageJ	Schneider et al., 2012	https://imagej.nih.gov/ij/
Code for heteromer quantification	this paper	Zenodo: https://doi.org/10.5281/zenodo.6975001
Other		
Dynabeads Protein A	Invitrogen	Cat#10002D
Dynabeads Protein G	Invitrogen	Cat#10004D

RESOURCE AVAILABILITY

Lead contact

Further information and requests for resources and reagents should be directed to and will be fulfilled by the lead contact, Bernd Fakler (bernd.fakler@physiologie.uni-freiburg.de).

Materials availability

Request for resources and reagents should be directed to lead contact.

Data and code availability

- The mass spectrometry proteomics data have been deposited to the ProteomeXchange Consortium via the PRIDE partner repository with the dataset identifier PXD036019 and https://doi.org/10.6019/PXD03601 and are publicly available as of the date of publication
- All original code has been deposited at GitHub and is available through https://doi.org/10.5281/zenodo.697500.
- Any additional information required to reanalyze the data reported in this paper is available from the lead contact upon request.

EXPERIMENTAL MODEL AND SUBJECT DETAILS

Animals

All experimental procedures were approved and performed in accordance with ethical regulations and the animal welfare committees of the Universities of Saarland and Freiburg. Every effort was made to minimize animal suffering and to reduce the number of animals used. The brains of the TRPC gene-deficient mouse lines TRPC1-/- (Dietrich et al., 2005, 2007), TRPC3-/- (Hartmann et al., 2008), TRPC4-/- (Freichel et al., 2001), TRPC5-/- (Xue et al., 2011), TRPC6-/- (Dietrich et al., 2005), and TRPC7-/- (Perez-Leighton et al., 2011) were taken from mixed male and female 9-22 week old adult mice bred for (Bröker-Lai et al., 2017; Camacho Londoño et al., 2015; Hartmann et al., 2008; Tsvilovskyy et al., 2009; Xue et al., 2011). The brains were snap-frozen and stored at -80°C in an organ repository. The generation of TRPC-IRES-Cre mouse strains and their breeding with eROSA26-τGFP to yield TRPC-IC/eR26- τGFP mice has been described (Schwarz et al., 2019; Wyatt et al., 2017).

Cell lines

tsA201 cells, a female human embryonic kidney cell-line, (96121229, identity confirmed by STR profiling, Sigma) were cultured at 37 °C, 5% CO_2 in Dulbecco's Modified Eagle's high glucose GlutaMAX medium (Gibco) supplemented with 10% fetal calf serum (Gibco), 1% penicillin/ streptomycin (Gibco) and 10 mM HEPES (Gibco). Stable cell lines expressing M2-type muscarinic receptors (HEK M2R) or co-expressing the receptors with TRPC5 (HEK TRPC5/M2R) were kindly provided by M. Zhu. Generation of the stable cell lines is described in (Miller et al., 2011). Cells were grown in DMEM (high glucose) supplemented with 10 % heat-inactivated FBS, 100 μg/ml Hygromycin B (M2R selection) and 400 μg/ml G418 (TRPC5 selection) at 37°C, 5% CO_2.

Primary cells

Primary hippocampal autaptic neuronal cultures, prepared from mixed male and female P0 mice, were grown for 10-17 days in NBA medium containing 2% B-27, 1% Glutamax and 1% penicillin/streptomycin at 5% CO_2 and 37°C.

Please cite this article in press as: Kollewe et al., Subunit composition, molecular environment, and activation of native TRPC channels encoded by their *interactomes*, Neuron (2022), https://doi.org/10.1016/j.neuron.2022.09.029

METHOD DETAILS

Antibodies

Commercially available antibodies: *anti*-TRPC4 (75-119, NeuroMab), *anti*-HA (11867423001, Roche) *anti*-GRM1a (610965, BD Biosciences), *anti*-GRM1 (SA-610, Biomol). All other antibodies summarized in Table S1 were generated in-house using peptides and recombinant protein fragments derived from individual TRPC proteins or INAM2 (Table S1) as immunogens and matrices for subsequent affinity purification of the antibodies (Flockerzi et al., 2005; Hirnet et al., 2003; Philipp et al., 2000).

Molecular biology

The cDNAs of mTRPC1 (Q61056), mTRPC4 (Q9QUQ5), TRPC5 (Q9QX29) and C-terminal HA-tagged GRM1 (P97772) were cloned by standard procedures. For electrophysiology, the cDNAs were subcloned into the plenti-hsynapsin lentiviral transfer vector or a eukaryotic expression vector peGFP-N1 (NovoPro), and YFP, CFP and mRFP were fused to the C-terminal ends. $TRPC5^{E418Q/E421Q/D439N}$ was generated by PCR using overlap expansion. All constructs were verified by DNA sequence analysis (Eurofins, Germany).

The HEK 293 cell line stably expressing the murine TRPC5 cDNA was generously provided by M. X. Zhu, Houston (Miller et al., 2011).

Generation of TRPC1-IRES-Cre and TRPC4-IRES-Cre mouse strains

TRPC1-IRES-Cre

The *IRES-Cre recombinase* cassette followed by a neomycin resistance gene (*neo*), flanked by consensus recombination sites of Flp recombinase (Flippase recognition target- or FRT-sites), was subcloned into a targeting vector 23 nucleotides 3' of the termination codon within the last protein-coding exon of *Trpc1* (Figure S3A). After electroporation of C57BL/6 ES cells, homologous recombination at the *Trpc1* locus was confirmed by Southern blot (Figure S3). Five targeted ES clones were expanded and karyotyped and three were injected into BALB/c blastocysts to generate the *Trpc1-IRES-Cre-neo+* mouse strain (F2 allele, Figure S3C). Following backcrossing chimeric animals with C57BL/6N wild-type, the offspring was bred to a Flp deleter mouse strain (Dymecki, 1996) to remove the neomycin resistance cassette from the *Trpc1* knockin allele. PCR genotyping confirmed successful removal of the neomycin resistance cassette (Figure S3D). One of the two ES cell-derived TRPC1-IC mouse lines was used for all further experiments.

TRPC4-IRES-Cre

To generate the TRPC4-IC mice, we produced an 8.2-kb targeting construct comprising a total of 4.7 kb of homologous sequence flanking an IRES-Cre-PGK-Neomycin cassette (Figure S4). The homologous stretches of DNA were generated by polymerase chain reaction (PCR), during which specific restriction sites were incorporated to enable assembly of the final construct by subsequent cloning steps. The IRES-Cre-PGK-Neomycin cassette is located 6 base pairs (bp) downstream of the stop codon, which is present in exon 11 of the Trpc4 gene. After sequence verification, the targeting construct was electroporated into mouse embryonic stem cells. Correctly targeted stem cells were injected into blastocysts to generate the TRPC4-IC knock-in mouse line. Flp recombinase deleter mice (Dymecki, 1996) were used to remove the neomycin resistance cassette. TRPC4-IC mice were genotyped using three primers (WTF: 5'-AGGTGGTGGTGGAAGACACC-3', WTR: 5'-TTGCCTGCCCAGAGCACTA-3', and NeoremF: 5'-AACTAAA CTGGTCGAGCGATGG-3') that produce two bands, 193 and 514 bp from the wild type and IRES-Cre alleles, respectively.

The breeding of TRPC1-IRES-Cre, TRPC4-IRES-Cre mice and TRPC5-IRES-Cre mice (Schwarz et al., 2019) with eROSA26-τGFP mice (Wen et al., 2011) to yield TRPC-IC/eR26- τGFP mice was performed as described (Schwarz et al., 2019; Wyatt et al., 2017).

Immunofluorescence staining of mouse brain sections

Animals were anesthetized with a mix of ketamine and xylazine and transcardially perfused with PBS followed by ice-cold 4% paraformaldehyde (PFA) in PBS. Brains were removed and post-fixed in ice-cold PFA for 2 hours, followed by overnight incubation in 18% sucrose at 4°C. Brains were frozen in freezing medium (OCT, Leica) and stored at -80°C until usage. Brains were sectioned (14 μm thick) on a cryostat (Leica), sections were stored at -80°C until usage. For immunofluorescence, sections were washed 3 times in PBS for rehydration at room temperature (RT) and then incubated in blocking solution (10% normal donkey serum (Jackson Immuno Research), 3% bovine serum albumin (Sigma) and 0.3% TX-100 (Roth)) for 1 hour at RT. Sections were incubated in primary antibody (chicken anti-GFP, 1:1000, #A10262 Invitrogen) overnight at 4°C. On the following day sections were washed 3 times in PBST (0.05% Tween-20 in PBS) and incubated in secondary antibody (goat anti-chicken 488, 1:500, #A11039 Invitrogen) for 2 hours at RT. Sections were washed in PBST and nuclei stained with bisbenzimide (Sigma). Sections were coverslipped in Fluoromount G (Southern Biontech) and stored at 4°C until imaging. Imaging was performed with the Axio Imager M2 (Zeiss).

Biochemistry

Transient transfection

For transient transfection, a mixture of plasmid DNA and polyethyleneimine (Polyscience) (ratio 2.5 to 1) in antibiotics-free culture medium was added to cells seeded one day before. For co-transfection TRPC1, TRPC4, TRPC5 and GRM1 plasmid DNAs were mixed at equal amounts.

Preparation of plasma membrane enriched protein fractions

Membrane fractions from brains of 5 to 6 week old rats (Wistar, Charles River, pools of 25 male and female rats each) or mice (WT: C57BL/6, Jackson Labs, pools of 25 male and female WT mice each, or two to three brains from TRPC knockout animals) were prepared as described (Kollewe et al., 2021). Extracted brains snap-frozen in liquid nitrogen were transferred into homogenization buffer (320 mM sucrose, 10 mM Tris/HCl pH 7.4, 1.5 mM $MgCl_2$, 1 mM EGTA and protease inhibitors (Leupeptin (Sigma), Pepstatin A (Sigma), Aprotinin (Roth) (1 μg/ml each), 1 mM Phenylmethylsulfonyl fluoride (Roth), 1 mM Iodoacetamide (Sigma)) cut into small pieces and homogenized in a dounce homogenizer. After removal of particulates (5 min, 1080 x g, 4 °C) homogenized material was collect by centrifugation (10 min, 200.000 x g, 4°C) and subjected to a 35 min hypotonic lysis (5 mM Tris/HCl pH 7.4 with protease inhibitors) with agitation on ice followed by centrifugation (10 min, 200,000 x g, 4°C). The pellet thoroughly resuspended in 0.5 M sucrose solution (sucrose, 10 mM Tris/HCl pH7.4, 1 mM EGTA) was layered on top of a 0.5 M and 3 M sucrose solution step gradient and centrifuged for 45 min at 123.000 x g, 4°C. The plasma membrane-enriched protein fraction was collected at the interface, diluted in 20 mM Tris/HCl pH 7.4, 1 mM EGTA, collected by centrifugation (20 min, 200,000 x g, 4 °C), and resuspended in 20 mM Tris/HCl, pH 7.4. Cultured cells were scraped off in phosphate-buffered saline solution with protease inhibitors 48 h after transfection, collected by centrifugation (5 min, 10,000 x g, 4 °C) and homogenized by sonication (2x 5 pulses, duty 50, output 2 (Branson Sonifier 250)) in homogenization buffer with protease inhibitors. After removal of particulates (10 min, 500xg), membranes were collected by centrifugation (20 min, 125,000 x g, 4 °C) and resuspended in 20 mM Tris/HCl pH 7.4. Protein concentrations were determined using the Bio-Rad Protein Assay Dye Reagent (Bio-Rad) according to manufacturer's instructions.

Blue-native polyacrylamide gel electrophoresis

Two dimensional polyacrylamide gel electrophoresis was performed as described by Schmidt et al. (2017). Plasma membrane-enriched protein fractions were solubilized on ice for 30 min in ComplexioLyte CL-47 at a protein to detergent ratio of 1:8 with added 1 mM EGTA and protease inhibitors. Solubilized material was cleared by centrifugation (7 min, 150.000 x g, 4 °C) and salts exchanged for aminocaproic acid by centrifugation through a sucrose step gradient (90 min, 415.000 x g, 4 °C). Samples were supplemented with 0.05 % Coomassie Blue G-250 and loaded onto non-denaturing 2-13% linear polyacrylamide gradient gels (anode buffer: 50 mM Bis-Tris, cathode buffer: 50 mM Tricine, 15 mM Bis-Tris, 0.02% Coomassie Blue G-250). For antibody-shift analyses, samples were incubated with *anti*-TRPC4/C5 (4/5A) antibody for 30 min on ice prior to poly-acrylamide gel electrophoresis. For denaturing analysis in the second dimension individual gel lanes were cut out, bathed in 2x Laemmli buffer for 10 min at 37 °C, and laid on top of SDS-polyacrylamide gels. Anti-TRPC4 (4A) and *anti*-TRPC5 (5D) were used for isoform-specific western-blot detection of TRPC4 and TRPC5, respectively. Native protein complexes visualized by total protein stains (SYPRO Ruby Protein Blot Stain, Bio-Rad) of the respective western blot membranes were used for alignment and molecular weight assignment.

Immunoprecipitation

Plasma membrane-enriched protein fractions were solubilized for 30 min on ice in ComplexioLyte CL-47 or CL-91 (Logopharm) supplemented with 1 mM EGTA and protease inhibitors at a protein to detergent ratio of 1:8. Solubilized material was cleared by centrifugation (10 min, 150,000 xg, 4 °C) and added to antibodies immobilized on Dynabeads (ThermoFisher Scientific). After 2 hrs of over-head incubation on ice, the unbound fraction was removed and Dynabeads were briefly washed with CL-47 or CL-91 dilution buffer (Logopharm). Precipitated proteins were eluted (10 min, 37 °C) in 1x Laemmli buffer with dithiothreitol added after elution and separated on SDS-polyacrylamide gels. For MS/MS analysis entire lanes of silver-stained gels (Heukeshoven and Dernick, 1988) were excised, split at 50 kDa, and pieces individually subjected to in-gel tryptic digests as described (Schmidt et al., 2017). For immunofluorescence detection, proteins were western blotted onto PVDF membranes (Immobilon) and probed with the following antibodies: *anti*-TRPC4/C5 (4/5E) or *anti*-HA (11867423001, Roche).

For serial APs, an equal mixture of two antibodies, both specifically targeting the same TRPC isoform, was used in each round to maximize AP efficiency. Antibody mixtures were *anti*-TRPC1: 1A+1B, *anti*-TRPC4: 4B+4C, *anti*-TRPC5: 5B+5C. In rounds two and three of serial APs the unbound protein fraction from the previous round was added to an immobilized antibody mixture not yet used in this series and incubated as before, so that *anti*-TRPC1, *anti*-TRPC4, and *anti*-TRPC5 APs were performed in every order possible providing a total of 15 eluates.

Mass spectrometry

Samples were analyzed either with an LC-MS system consisting of a split-based UltiMate 3000 HPLC (Dionex, now Thermo Fisher Scientific), a Proxeon nanospray ion source, and an LTQ Orbitrap XL hybrid ion trap-orbitrap mass spectrometer (Thermo Fisher Scientific) or with an LC-MS system consisting of a split-free UltiMate 3000 RSLCnano HPLC, a Nanospray Flex ion source, and a Q Exactive HF-X hybrid quadrupole-orbitrap mass spectrometer (all Thermo Fisher Scientific).

LTQ Orbitrap XL analyzed samples were processed in the following way: Vacuum-dried tryptic peptides were dissolved in 0.5% trifluoroacetic acid, partially loaded onto a trap column (C18 PepMap100, 5 μm particles, Thermo Fisher Scientific) with 0.5% acetic acid (5 min, 20 μL/min) and separated on a C18 reversed phase column (SilicaTip™ emitter, 75 μm i.d., 8 μm tip, New Objective, manually packed 12 cm with ReproSil-Pur ODS-3, 3 μm particles, Dr. A. Maisch HPLC; flow rate: 300 nL/min). The aqueous-organic gradient was formed with eluent A (0.5% (v/v) acetic acid in water) and eluent B (0.5% (v/v) acetic acid in 80% (v/v) acetonitrile / 20% (v/v) water): 5 min 3% B, 60 min from 3% B to 30% B, 15 min from 30% B to 100% B, 5 min 100% B, 5 min from 100% B to 3% B, 15 min 3% B (flow rate: 300 nL/min). Eluted peptides were electrosprayed at 2.3 kV (positive ion mode) into the mass spectrometer and analyzed by data-dependent acquisition. Each scan cycle consisted of one Orbitrap precursor scan (scan range 370 to

1700 m/z; nominal resolution 60,000 (FWHM) at m/z 400; AGC target 500,000) and up to five ion trap MS/MS scans ("TOP5"; AGC target 10,000; maximum injection time 400 ms; dynamic exclusion 30.0 s (± 20 ppm); preview mode for FTMS master scans, charge state screening, and monoisotopic precursor selection enabled; charge state 1 rejected; minimum signal threshold 1,000 counts; isolation width 2.0 m/z; default CID activation parameters). Peak lists were generated with ProteoWizard msConvert (http://proteowizard.sourceforge.net/; version 3.0.6906), linear shift mass recalibrated (after a preliminary database search with high mass tolerance) with an in-house developed script, and finally searched against all mouse, rat, and human entries of the UniProtKB/Swiss-Prot database with Mascot Server 2.6.2 (peptide mass tolerance ± 5 ppm, fragment mass tolerance ± 0.8 Da; Kollewe et al., 2021). For successful identification of mouse InaF-motif-containing protein 2 UniProtKB/TrEMBL sequences A0A1L1STD6, as well as NCBI reference sequence XP_017447683.2 were added to the database.

Q Exactive HF-X analyzed samples were processed similarly with the following differences: Peptides were loaded onto the trap column with 0.05% trifluoroacetic acid (4 min, 10 μL/min). The packed bed of the analytical column was 23 cm long. The following gradient was used: 5 min 3% B, 60 min from 3% B to 30% B, 10 min from 30% B to 40% B, 5 min from 40% B to 50% B, 5 min from 50% B to 99% B, 5 min 99% B, 5 min from 99% B to 3% B, 10 min 3% B. Each scan cycle consisted of one precursor scan (scan range 370 to 1700 m/z; nominal resolution 240,000 (FWHM) at m/z 200; AGC target 3,000,000) and up to ten data-dependent MS/MS scans ("TOP10"; HCD fragmentation of doubly, triply and quadruply charged ions; nominal resolution 15,000 (FWHM); AGC target 100,000; maximum injection time 200 ms; isolation window 1.0 m/z; fixed first mass 100.0 m/z; normalized collision energy 28; minimum AGC target 8,000; peptide match preferred; isotopes excluded; dynamic exclusion 30.0 s (± 10 ppm)). The ProteoWizard version was 3.0.11098, and final Mascot searches were performed with a fragment mass tolerance of ± 20 mmu.

Quantitative evaluation

Label-free quantification of proteins was based on peptide LC-MS signal intensities (peak volumes, PVs) that were obtained from FT full scans mass calibrated offline using MaxQuant v1.6.3 (http://www.maxquant.org). Peptide PV elution times in each dataset were then pairwise aligned using LOESS regression (the reference times were dynamically calculated from the median peptide elution times over all datasets already aligned) and then assigned to peptides obtained directly or indirectly from MS/MS-identification (based on congruent m/z and elution times, tolerance 2-3 ppm / ± 1 min) as described (Bildl et al., 2012). Next, the impact of missed or incorrectly assigned peptide PVs was reduced by applying a newly developed procedure. First, accuracy of peptide PVs was determined by analyzing matrices of protein-specific peptide PVs (peptides vs runs) for *internal consistency* between MS-runs and with regard to the relative peptide ionization efficiencies (i.e. by calculating ''expected PV values'' (ePVs)). Second, time- and run-dependent detectability thresholds were estimated for each of the PV matrix cells (peptide/run pairs) based on the 3rd percentile of PV values from peptides co-eluting within a 3 minutes time window. Third, global protein models ('protein reference ridges') were established by aggregation of protein-specific peptide PV values from qualified datasets (i.e. with highest coverage of the respective proteins). These protein reference ridges reflected the maximum protein coverage of MS/MS-identified and quantified peptides with their relative ionisation efficiencies and allowed for conversion into molecular abundances (abundance$_{norm}$spec values) as described (Bildl et al., 2012). Finally, quantification of proteins was achieved by weighted fitting of their measured PVs in each dataset to the respective reference ridges. In case no (consistent) peptide PVs could be identified, the detectability thresholds of the three best ionizing peptides were fitted instead.

To determine specificity in affinity purifications (APs), ratios of molecular abundances of proteins in wt versus control APs were calculated, logarithmized (basis 10) and normalized to the abundance ratio of the respective target (= maximum 100%) and to the estimated distribution of the background proteins (= minimum 0%). The resulting target-normalized ratios (tnRs) and molecular abundances were collectively inspected using the BELKI software suite (https://github.com/phys2/belki) suggesting the following criteria for specific and consistent co-purification with TRPC channels: TRPC1/4/5 CL-91: tnR >0.3 in at least four APs, >0.25 in at least five APs, or >0.2 in at least six APs; TRPC1/4/5 CL-47: tnR >0.3 in at least four APs, or >0.2 in at least five APs; TRPC6 CL-91: tnR >0.35 in at least two APs; TRPC7 CL-91: tnR >0.3 in both APs; TRPC7 CL-47: tnR >0.35 in both APs. Only tnR values with a confidence score below 0.55 were considered, and only, if the protein's molecular abundance was high enough so that its log-space enrichment over threshold in the WT sample was at least 1.5 times its enrichment over threshold in the control sample + 0.25 (orders of magnitude). DNA and RNA-binding proteins were removed manually. The results of the automated analysis were thoroughly manually rechecked, and based on the available primary data (peak volumes) proteins either accepted or discarded as specific TRPC interactors.

Determination of heteromer composition from serial APs

First, to correct for variations in protein input, protein abundances in all samples obtained with the same antibody mixture were normalized using those proteins as a common reference that were exclusively, but TRPC-independently, co-purified with that antibody mixture due to antibody cross-reactivities. Second, the relative amount of each TRPC isoform in each AP was calculated with respect to its total amount in the respective AP series. Third, relative TRPC protein amounts from rounds two and three were used to determine AP efficiencies in rounds one and two. AP efficiency was 74% to 84% for TRPC1 in *anti*-C1 APs, 95% to 100% for TRPC4 in *anti*-C4 APs, and 87% to 92% for TRPC5 in *anti*-C5 APs. Fourth, the amount of each TRPC isoform in each AP was expressed as a linear equation and defined as the sum of its amounts in all homo- and heteromers that could have been precipitated in this AP, multiplied by the precipitation efficiency, including homo- and heteromers that had not been

Please cite this article in press as: Kollewe et al., Subunit composition, molecular environment, and activation of native TRPC channels encoded by their *interactomes*, Neuron (2022), https://doi.org/10.1016/j.neuron.2022.09.029

precipitated in previous rounds of the same AP series due to non-depleting precipitation. The allocation of each TRPC isoform to all possible homo- and TRPC1/C4/C5 heteromers was finally calculated by solving the resultant overdetermined system of 15 linear equations for each TRPC isoform using a bound least squares solver. Quantification of serial APs with TRPC1$^{-/-}$, TRPC4$^{-/-}$ or TRPC5$^{-/-}$ membrane fractions was done as described for wild-type, providing four linear equations for each remaining TRPC isoform per TRPC knockout membrane fraction.

Electrophysiology

Chemicals

Hygromycin B, G418, CNQX, Picrotoxin, Bicuculline, Englerin A, B-27 and U-72122 were purchased from Sigma-Aldrich (Germany). TTX was supplied from Abchem. D-AP5 and DHPG (RS)-3,5 were from Tocris. BAPTA, tetrapotassium salt, Plyronic acid (F-127), Fetal Bovine Serum, penicillin/streptomycin, Glutamax, DMEM and Neurobasal media were purchased from Invitrogen. Fura-2 AM was purchased from Thermo-Fisher.

Cell lines, primary cell culture and transfection

Primary hippocampal autaptic neurons were prepared as previously described in Schwarz et al. (2019). Briefly, neurons were prepared from age matched TRPC1,C4,C5 triple-knockout (Bröker-Lai et al., 2017), TRPC-IC/eR26- τGFP and wt P0-P1mice (C56Bl/6N strain) and cultured on astrocytic microislands (Schwarz et al., 2019). Autaptic cultures were grown for 10-17 days in NBA medium containing 2% B-27, 1% Glutamax and 1% penicillin/streptomycin at 5% CO_2 and 37°C. HEK M2R and HEK TRPC5/M2R cells seeded on 25 mm PDL-coated (0.5 mg/ml, Sigma-Aldrich, Germany) glass coverslips were transfected 20-26 h prior to the experiment using Lipofectamine 2000 (Invitrogen) according to the manufacturer's protocol. Transfected cells were identified by their reporter fluorescence.

Patch clamp recordings

Electrophysiological recordings of HEK293 cells were performed in extracellular solution (ECS), containing (in mM) 130 NaCl, 10 CsCl, 2 $MgCl_2$, 1 $CaCl_2$, 10 HEPES, 10 Glucose, pH 7.3, 300-310 mOsm. The patch pipette solution contained (in mM) 120 CsCl, 10 NaCl, 3 $MgCl_2$, 0.1 EGTA or 10 BAPTA, 10 HEPES, pH 7.3 (with CsOH), 280-290 mOsm. Englerin A (30 nM) and DHPG (100 μM) were locally applied by gravity flow. Recording pipettes had a resistance of 2.5-4 MΩ. Inward currents were measured in the voltage-clamp mode at -70 mV in extracellular solution containing (in mM): 120 NaCl, 2.6 KCl, 1-2 $CaCl_2$, 2 $MgCl_2$, 20 HEPES, 30 Glucose, pH 7.3, 290-300 mOsm. To isolate DHPG-induced currents, the extracellular solution was supplemented with (in μM): 30 Picrotoxin, 10 CNQX, 10 Bicuculline, 10 D-AP5, 1 TTX. The intracellular patch pipette solution contained (in mM): 140 K-Gluconate, 11 NaCl, 2 Mg-ATP, 0.2 Na_2-GTP, 1.1 EGTA, 11 HEPES, 11 Glucose, 280 mOsm (pH 7.3 with NaOH). Recordings were performed with an EPC10 amplifier (HEKA Electronic, Germany) and controlled by Pulse 8.5 program (HEKA Electronic, Germany). Only cells with an access resistance of 5-15 MΩ, 60-80 % resistance compensation and a leak current of <100 pA (for HEK293 cells) or <300 pA (for neurons) were analysed. Electrophysiological measurements were recorded at the digitalization rate of 20 kHz and analysed using customized routine in IgorPro (Wavemetrics, USA).

Electrophysiological recordings from giant inside-out patches excised from *Xenopus* oocytes injected with TRPC4 and TRPC1/C4/C5-specific cRNAs were performed at room temperature (22-24 °C) as described (Schwenk et al., 2012). Briefly, currents were recorded with an EPC10 amplifier, low-pass filtered at 3 kHz, and sampled at 5-10 kHz. Pipettes made from thick-walled borosilicate glass had resistances of 0.4-0.8 MΩ when filled with extracellular (pipette) solution (in mM) 120 NMDG-MES, 1 KCl, 10 HEPES, 5 EGTA, pH adjusted to 7.2. Intracellular solution was (mM): 110 K-MES, 10 Na-MES, 5 HEPES, 10 EGTA (pH 7.2). CaMES was added to obtain free [Ca^{2+}] concentrations of 0.1 μM, 0.3 μM, 1 μM, 3 μM and 10 μM. For calculation of the appropriate amount of Ca^{2+} to be added WEBMAXC STANDARD (https://somapp.ucdmc.ucdavis.edu/pharmacology/bers/maxchelator/webmaxc/webmaxcS.htm) was used, final free Ca^{2+}-concentrations were checked with a Ca^{2+}-sensitive electrode (World Precision Instruments, Sarasota, USA). Rapid application/removal of Ca^{2+} was performed using a Piezo-controlled fast application system with a double-barrel application pipette that enables solution exchanges within less than 100 μs (20-80%, measured from the open tip response).

Data are given as means ± SEM throughout the manuscript. Significance was assessed by non-parametric Mann-Whitney U-test.

QUANTIFICATION AND STATISTICAL ANALYSIS

All statistical details are indicated in the STAR Methods and/or in the figure legends. Data are given as means ± SEM throughout the manuscript. Significance was assessed by non-parametric Mann-Whitney U-test. Significance levels are indicated (***, ** and * for p-values of < 0.001, 0.01 and 0.05, respectively).